


RESEARCH ARTICLE

# Susceptibility to diet-induced obesity at thermoneutral conditions is independent of UCP1

Sebastian Dieckmann,<sup>1,2,3</sup> Akim Strohmeyer,<sup>1,2,3</sup> Monja Willershäuser,<sup>1,2,3</sup> Stefanie F. Maurer,<sup>1,2,3</sup> Wolfgang Wurst,<sup>4,5,6</sup> Susan Marschall,<sup>7</sup> Martin Hrabe de Angelis,<sup>7,8,9</sup> Ralf Kühn,<sup>4</sup> Anna Worthmann,<sup>10</sup> Marceline M. Fuh,<sup>10</sup> Joerg Heeren,<sup>10</sup> Nikolai Köhler,<sup>11</sup> Josch K. Pauling,<sup>11</sup> and  Martin Klingenspor<sup>1,2,3</sup>

<sup>1</sup>Chair for Molecular Nutritional Medicine, TUM School of Life Sciences, Technical University of Munich, Freising, Germany;

<sup>2</sup>EKFZ - Else Kröner Fresenius Center for Nutritional Medicine, Technical University of Munich, Freising, Germany; <sup>3</sup>ZIEL -

Institute for Food & Health, Technical University of Munich, Freising, Germany; <sup>4</sup>Institute of Developmental Genetics,

Helmholtz Zentrum München, Germany; <sup>5</sup>TUM School of Life Sciences, Technical University of Munich, Freising, Germany;

<sup>6</sup>German Center for Neurodegenerative Diseases (DZNE), Site Munich, Germany; <sup>7</sup>Institute of Experimental Genetics,

Helmholtz Zentrum München, Neuherberg, Germany; <sup>8</sup>Chair of Experimental Genetics, TUM School of Life Sciences,

Technical University of Munich, Freising, Germany; <sup>9</sup>German Center for Diabetes Research (DZD), Neuherberg, Germany;

<sup>10</sup>Department of Biochemistry and Molecular Cell Biology, University Medical Center Hamburg-Eppendorf, Hamburg,

Germany; and <sup>11</sup>LipiTUM, Chair of Experimental Bioinformatics, TUM School of Life Sciences, Technical University of Munich, Freising, Germany

## Abstract

Activation of uncoupling protein 1 (UCP1) in brown adipose tissue (BAT) upon cold stimulation leads to substantial increase in energy expenditure to defend body temperature. Increases in energy expenditure after a high-caloric food intake, termed diet-induced thermogenesis, are also attributed to BAT. These properties render BAT a potential target to combat diet-induced obesity. However, studies investigating the role of UCP1 to protect against diet-induced obesity are controversial and rely on the phenotyping of a single constitutive UCP1-knockout model. To address this issue, we generated a novel UCP1-knockout model by Cre-mediated deletion of exon 2 in the *UCP1* gene. We studied the effect of constitutive UCP1 knockout on metabolism and the development of diet-induced obesity. UCP1 knockout and wild-type mice were housed at 30°C and fed a control diet for 4 wk followed by 8 wk of high-fat diet. Body weight and food intake were monitored continuously over the course of the study, and indirect calorimetry was used to determine energy expenditure during both feeding periods. Based on Western blot analysis, thermal imaging and noradrenaline test, we confirmed the lack of functional UCP1 in knockout mice. However, body weight gain, food intake, and energy expenditure were not affected by loss of UCP1 function during both feeding periods. We introduce a novel UCP1-KO mouse enabling the generation of conditional UCP1-knockout mice to scrutinize the contribution of UCP1 to energy metabolism in different cell types or life stages. Our results demonstrate that UCP1 does not protect against diet-induced obesity at thermoneutrality.

**NEW & NOTEWORTHY** We provide evidence that the abundance of UCP1 does not influence energy metabolism at thermoneutrality studying a novel Cre-mediated UCP1-KO mouse model. This model will be a foundation for a better understanding of the contribution of UCP1 in different cell types or life stages to energy metabolism.

*adipose tissue; diet-induced obesity; thermogenesis; uncoupling protein 1*

## INTRODUCTION

Thermogenic brown adipose tissue (BAT) is the main contributor to nonshivering thermogenesis, a key process to maintain normothermia in a variety of small mammals. Nonshivering thermogenesis is mediated by the uncoupling protein 1 (UCP1), which enables high rates of oxygen consumption by the mitochondrial electron transport chain without ATP production. Cold exposure elicits the most

potent stimulation of UCP1-mediated uncoupled respiration for thermoregulatory nonshivering thermogenesis (1). The effect of cold is conveyed by a well-established somatosensory reflex activating the sympathetic innervation of BAT. The neurotransmitter norepinephrine triggers  $\beta$ -3-adrenergic receptor signaling in brown adipocytes, which acutely activates lipolysis and UCP1-mediated uncoupled respiration, fueled by the uptake of glucose, fatty acids, and triglyceride-rich lipoproteins from the circulation (2). During cold

acclimation, chronic elevation of the sympathetic tone in BAT results in the massive recruitment of mitochondrial biogenesis and the transcriptional signature of the thermogenic machinery. Recruitment of thermogenic capacity in BAT not only occurs during cold acclimation but also in response to caloric overfeeding. The latter stimulates the sympathetic tone in BAT and increases the expression of UCP1 in brown adipocytes (3). It has been proposed, that BAT thereby lowers metabolic efficiency, known as *luxusconsumption*, or diet-induced thermogenesis, resulting in elevated daily energy expenditure at rest and less body fat accumulation than expected from ingested calories (4).

Other than diet-induced thermogenesis, meal-associated thermogenesis represents the transient rise in resting metabolic rate during and after a meal, also known as the thermic effect of feeding or specific dynamic action. Mechanistically, meal-associated thermogenesis is caused by obligatory ATP-dependent processes related to food ingestion, digestion, absorption, and anabolic pathways, and facultative (adaptive) mechanisms like meal-associated activation of BAT thermogenesis (5). Recent reports demonstrate that the prandial surge of the gut peptide hormone secretin elicits BAT activation in mouse (6) and in man (7). Notably, within individuals, cold-induced and meal-associated activation of BAT are not associated, indicating differential mediators and functions (8). Other activators of thermogenesis have been reported (9, 10) and recent findings suggest brown fat effects on systemic metabolism and energy balance by means of paracrine intercellular and endocrine interorgan cross talk (11). Activation of BAT has beneficial cardiometabolic effects (12) due to more than the mere combustion of calories (13). Together with the potential of BAT to impact energy balance and systemic metabolism by clearing glucose and lipids from circulation, these characteristics render UCP1 and BAT potential targets to improve cardiometabolic health and the treatment of type 2 diabetes (12).

In this context, the question whether UCP1 can protect against diet-induced obesity (DIO) has been studied repeatedly (see Table 1 for an overview). Standard housing temperature (20°C–23°C) represents a cold challenge for laboratory mice resulting in a twofold increase of daily energy expenditure (14). BAT is the source for this thermoregulatory heat production. UCP1 knockout mice when kept at standard housing temperature do not develop DIO (15) and even seem to be protected, having lower body weight than WT mice (16–18). It remains unresolved whether and how this DIO resistance in UCP1-KO mice may be related to alternative nonshivering thermogenic mechanisms and/or muscle shivering to cope with the need for thermoregulatory heat production. Housing mice at higher ambient temperatures (27°C–30°C), corresponding to their thermoneutral zone, eliminates this heat sink. Caloric overfeeding mice with high-fat diets (HFDs), Western type diets, or Cafeteria diets results in a moderate increase of UCP1 gene expression in BAT but it remains to be resolved whether the underlying increase in sympathetic tone at thermoneutrality also sufficiently triggers UCP1 activation to affect whole body energy expenditure.

Here, another level of complexity comes into play, as dietary interventions alter the gut microbiota composition with meanwhile numerous studies investigating how such

changes influence host metabolism (19). Systemic cross talk via a microbiota-liver-BAT axis was suggested to convey DIO resistance in the cold (20), and microbiota effects on BAT and brown-like brite/beige adipocytes in white adipose tissues have been reported, however, with conflicting results. Colonization of conventional mice with specific bacterial strains induced UCP1 expression (21). Fecal transfer of gut microbiota from cold-exposed mice increased UCP1 expression in BAT and white adipose tissue (22) but this was not confirmed in a related study (23). Intermittent fasting can induce the recruitment of brown/brite adipocytes in white adipose tissue (24). Inversely, these findings imply that UCP1 ablation resulting in impaired BAT thermogenesis of the host may impact gut microbiota composition and trigger microbiota-associated alterations in lipid metabolism. In that case, differences between housing facilities in gut microbiota of mice may also influence their metabolic phenotypes, like DIO susceptibility.

No consequences for energy balance should occur without UCP1 activation. Indeed, several studies using the established UCP1-KO mouse model, originally generated by Leslie Kozak and coworkers, confirmed this expectation (10, 17, 25–28) (Table 1). In contrast, other studies reported that UCP1 knockout mice are more susceptible to diet-induced obesity at thermoneutrality (29–33) (Table 1). One explanation for the increased susceptibility to DIO in UCP1-KO mice may be increased metabolic efficiency, defined as a larger gain of body fat mass per unit of metabolizable energy, due to the lack of diet-induced BAT thermogenesis in UCP1-KO mice (31). However, recent data from a UCP1 knockdown model (34) demonstrate that UCP1 abundance alone does not protect against DIO at thermoneutrality. Despite having remarkable reduced but still inducible UCP1 expression levels, these mice are not more or less prone to DIO compared with wild-type (WT) littermates with high-fat diet-induced elevation in UCP1 expression.

Taken together, this showcases the urgent need for new UCP1-KO models to scrutinize the role of UCP1 on energy balance and metabolism. So far two UCP1 knockout models are available (15, 26). Other transgenic mice with impaired UCP1 expression include knockdown models (35, 36) or diphtheria toxin chain A-induced depletion of UCP1 expressing cells (37, 38). In the present study, we therefore introduce and validate a novel Cre-mediated UCP1-KO model and demonstrate that deletion of UCP1 in this model has no effect on energy balance regulation at thermoneutrality.

## MATERIAL AND METHODS

### Animal Model

The UCP1 knockout mouse line was generated in frame of the EUComm program and is a constitutive UCP1 knockout model on a C57BL/6N background (39, 40). It originates from the *Ucp1<sup>tm1a</sup>* mouse (C57BL/6N), carrying a *lacZ* and *neomycin (neo)* cassette, two *FRT* sites, and three *loxP* sites (Fig. 1A). Through crossing with a flippase (Flp) mouse (C57BL/6N), the *lacZ* and *neo* cassette as well as one *FRT* site and one *loxP* site were removed, resulting in the *Ucp1<sup>tm1c</sup>* mouse (UCP1-WT). Crossbreeding this mouse with a *Rosa26-Cre* mouse (C57BL/6N) results in the *Ucp1<sup>tm1d</sup>* mouse (UCP1-KO)

**Table 1.** Overview of studies investigating the effect of HFD at thermoneutrality in the conventional UCP1-KO model (26)

Study	Strain	Sex	Caging	Ambient Temperature, °C		Diet(s), %kcal/fat	Age at HFD start (wk)	Feeding Period(wk)	Effects KO vs. WT								
				Pre	Exp.				BM	BMchange	FM	WAT	FI	EI	ME	RQ	RMR
Enerbäck (26)	Mixed 129/SvPas-C57BL/6J	m/f	n.a.	n.a.	n.a.	HFD (?)	8*	12*	±		±			n.a.			
Liu(17)	C57BL/6J	m	single	27	20 → 27	HFD (58)	8*	20	± <sub>start</sub>	↓ <sub>20°C</sub>				±			
					20	HFD (58)	8*	8	± <sub>end</sub>	↓ <sub>30°C</sub>				±			
					27	HFD (58)	12*	2	↓			↓				± <sub>mean</sub> ↓ <sub>PRCF</sub>	
Anunciado-Koza(25)	C57BL/6J	m	single	20	20 → 28	HFD (58)	10–12	10 <sub>at 20°C</sub> → 10 <sub>at 28°C</sub>	±	↓ <sub>20°C</sub> ± <sub>30°C</sub>	±		↓				
Feldmann (29)	C57BL/6	m	single	n.a.	29	HFD (45)	n.a.	16*		↑		↑	↑		↑		±
Rowland(30)	C57BL/6J	n.a.	n.a.	29	29	HFD (45)	10	12		↑		↑		±	↑	±	
Zietak(10)	C57BL/6J	m	Group	29	29	HFD (58)	8	9		±	±			±			
Von Essen(31)	C57BL/6	m	Single	21	30	HFD (45)	12-16	4	±	↑	↑			↓	↑		
Winn(28)	C57BL/6J	f	Pairs	n.a.	25	WD (45)	6	28	±		±			±	±	±	
Luijten(32)	129S2/sv	m	Single	n.a.	30	HFD (45)	10–14	1*		↑	±	↑		±	↑	±	
Maurer(27)	129SV/pas	m	Single	n.a.	30	HFD (45)	6–9	1*		↑	↑ <sub>change</sub>			±			±
	C57BL/6J	m	Group	23	30	CD (13)	10–14	4 <sub>CD</sub> →	± <sub>CD</sub>		± <sub>CD</sub>			± <sub>CD</sub>			
						IFD (31)	± <sub>IFD</sub>		± <sub>IFD</sub>			± <sub>IFD</sub>					
						HFD (48)	± <sub>HFD</sub>		± <sub>HFD</sub>			± <sub>HFD</sub>					
	C57BL/6J							± <sub>CD</sub>		± <sub>CD</sub>			± <sub>CD</sub>				
								± <sub>IFD</sub>		± <sub>IFD</sub>			± <sub>IFD</sub>				
	129S1/SvImJ								↓ <sub>HFD</sub>		↓ <sub>HFD</sub>			↓ <sub>HFD</sub>			
								± <sub>CD</sub>		± <sub>CD</sub>			± <sub>CD</sub>				
Pahalavani(33)	C57BL/6J	m	n.a.	n.a.	28–30	HFD (45%)	5–6	14	± <sub>IFD</sub>		± <sub>IFD</sub>			± <sub>IFD</sub>			

Effects expressed as significantly decreased (↓), increased (↑), or not significantly altered (±) in UCP1 knockout (KO) compared with wild-type (WT) mice. Information was not provided in the original publication (n.a.), temperature before the start of the study (pre) and during the experiment (exp.), high-fat diet (HFD), control diet (CD), intermediate fat diet (IFD), body mass (BM), body mass change (BM<sub>change</sub>), fat mass (FM), white adipose tissue (WAT), food intake (FI), energy intake (EI), metabolic efficiency (ME), respiratory exchange ratio (RQ), and resting metabolic rate (RMR), percent relative cumulative frequency (PRCF). \*Values that were recalculated, as they were stated in a different measure in the original publication. Sequential study designs are indicated by a right arrow (→).

carrying a germline deletion of exon 2 in the *Ucp1* gene. UCP1-KO and UCP1-WT mice were crossed to generate heterozygous UCP1-HET mice. The UCP1 knockout line is maintained by crossing male and female UCP1-HET mice. All studied mice were derived of our heterozygous maintenance breeding. Mice were bred and housed at 23°C ambient temperature with a 12/12-h light/dark cycle and had ad libitum access to water and chow diet.

All animal experiments were performed according to the German animal welfare law and approved by the district government of Upper Bavaria (Regierung von Oberbayern, Reference No. ROB-55.2–2532.Vet\_02–15–128).

#### HFD feeding at thermoneutrality.

Male wild-type ( $n = 7$ ) and knockout ( $n = 7$ ) mice for the high-fat diet feeding experiment were obtained from our heterozygous maintenance breeding. At the age of 8 wk, mice were switched from chow to a chemically defined control diet (CD) with a fat content of 50 g/kg (CD, ~13 kJ% from fat, 15.3 MJ/kg, Sniff Cat. No. S5745-E702). Simultaneously, mice were single caged and transferred to climate cabinets with an ambient temperature of 30°C and 55% RH. After an acclimatization phase of 4 wk, mice were switched from CD to a high-fat diet with a fat content of 250 g/kg (HFD, ~48 kJ% from fat, 19.6 MJ/kg, Sniff Cat. No. S5745-E712). After 8 wk of HFD feeding, mice were killed by CO<sub>2</sub> asphyxiation. Whole blood was taken by cardiac puncture, collected in lithium

heparin-coated tubes (Sarstedt, Nümbrecht, Germany), and centrifuged at 4°C for 10 min with 1,500 g. The plasma supernatant was transferred to fresh tubes and snap frozen in liquid nitrogen. Subsequently, cecal content and tissues were dissected, weighed, and immediately snap frozen in liquid nitrogen. Cecal content, tissues, and plasma were stored at –80°C until further processing. Body weight and food intake were determined twice a week between 12:00 PM and 4:00 PM. In addition, body composition was determined every other week by nuclear magnetic resonance spectroscopy (mq7.5, Bruker BioSpin GmbH, Rheinstetten, Germany). Mice were maintained on a 12/12-h light/dark cycle and had ad libitum access to water and the respective diets during the whole experiment. Food was replaced completely twice a week to avoid rancidity of the HFD at 30°C.

#### Indirect Calorimetry, Basal Metabolic Rate, and Noradrenaline Tests

Indirect calorimetry was performed based on an open respirometer system (LabMaster System; TSE Systems, Bad Homburg, Germany), similar to previously described methodology (41). O<sub>2</sub> consumption and CO<sub>2</sub> production were determined after 2.5 wk of feeding CD and after 4 wk of HFD. Mice were transferred in specially equipped cages in a climate cabinet (KPK 600, Feutron, Germany) set to 30°C after determining body weight and body composition in the afternoon (2:00–5:00 PM). The measurement was started on the next day at 6:00 AM

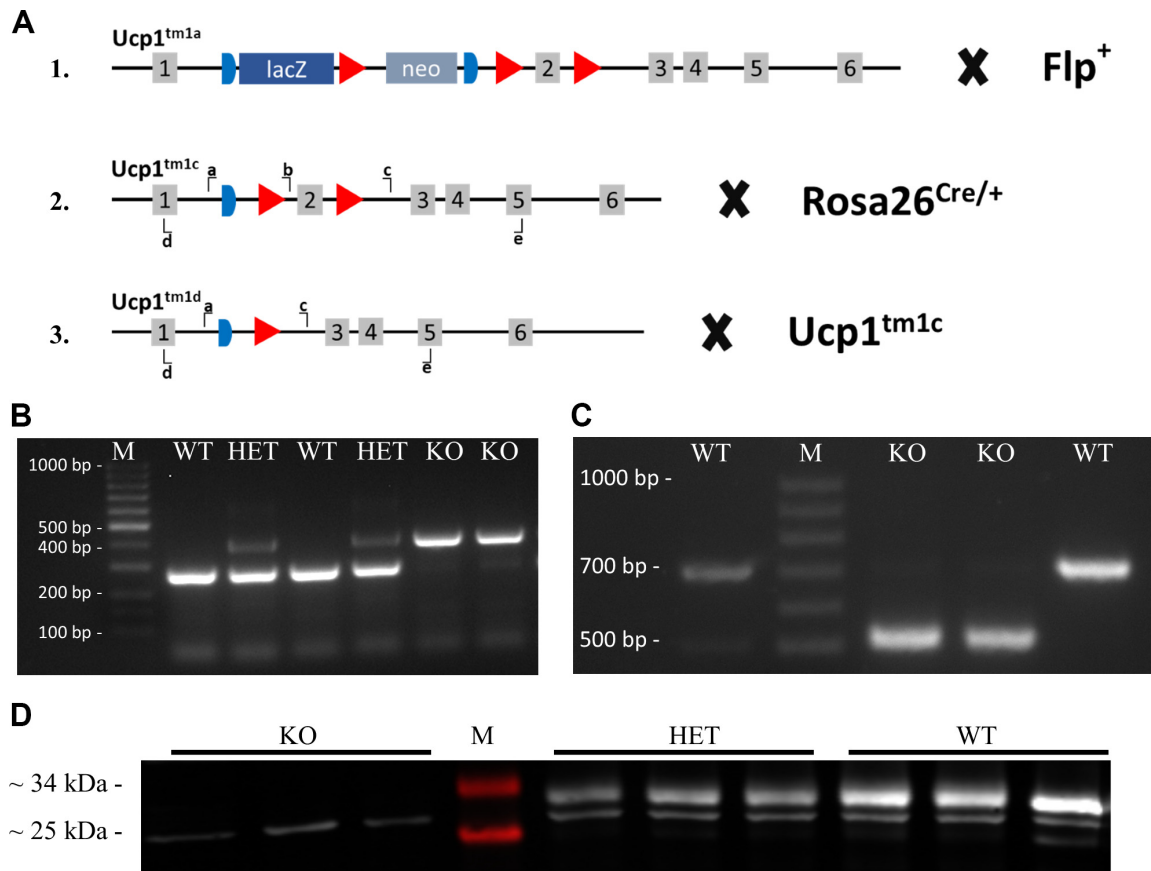


**Figure 1.** Overview and validation of the *Ucp1* knockout strategy. **A:** breeding scheme for the generation of the *Ucp1* knockout. All mice were on a C57BL/6N background. **A1:** *Ucp1<sup>tm1a</sup>* mice containing three *loxP* sites (red), two *FRT* sites (blue) as well as a *lacZ* and a *neomycin* (*neo*) cassette were crossed with mice expressing flippase (*Flp<sup>+</sup>*). **A2:** mice with the resulting *Ucp1<sup>tm1c</sup>* allele [wild-type (WT)] were crossed with a *Rosa26<sup>Cre/+</sup>* mouse, deleting exon 2 of the *Ucp1* gene, generating the *Ucp1<sup>tm1d</sup>* [knockout (KO)] allele. **A3:** *Ucp1<sup>tm1c</sup>* (WT) and *Ucp1<sup>tm1d</sup>* (KO) mice were crossed to generate mice heterozygous (HET) for the knockout allele. Lower case letters indicate binding positions of primers used for PCR (a–c) and RT-PCR (d and e). **B:** PCR of gDNA from tissue samples of WT, HET, and KO mice. **C:** RT-PCR products from iBAT of WT and KO mice. **D:** representative Western blot analysis for UCP1 (~33 kDa) in KO, HET, and WT mice. See Supplemental Fig. S2 for the uncropped image. iBAT, interscapular brown adipose tissue; KO, knockout.

(CD) or 12:00 PM (HFD) and continued two (CD) or three (HFD) dark phases. The air from the cages was extracted over a period of 1 min every 4–6 min. Heat production was calculated according to Heldmaier (42) as:  $HP [mW] = (4.44 + 1.43 \times \text{respiratory exchange ratio}) \times \text{oxygen consumption [mL/h]}$ .

Basal metabolic rate (BMR) was determined immediately after the last night phase of the indirect calorimetry measurement of the HFD period. Mice were deprived of food between 7:00 and 8:00 AM for at least 4 h. BMR was calculated as the mean of the four lowest consecutive heat production measurements during the last 90 min of fasting, similar to a previously published method (43). Subsequently, noradrenaline tests were performed between 10:00 AM and 5:00 PM at 26°C to avoid noradrenaline-induced hypothermia. Noradrenaline (1 mg/kg, Arterenol, Sanofi) was injected intraperitoneally. Air was extracted continuously from the cages with a measurement period of 1 min over 60 min.

#### Collection of Food Spillage and Feces

Embedding material was collected from cages after indirect calorimetry for each mouse separately to correct food intake for spillage and to determine energy loss by fecal

excretion. Material was dried at room temperature under a chemical flow hood for at least 1 wk. Subsequently, cage material was fractionated based on size by shaking the material on a sieve shaker (EML 200 Digital Plus T, Haver & Boecker, Oelde, Germany) for 5 min with an interval of 0.5 min at an amplitude of 1.4, through sieves with different mesh sizes (4, 3.15, 2.5, 1.25, and 1 mm, VWR International GmbH, Darmstadt, Germany). Flowthrough of the 1-mm sieve was collected in a pan. Each sieve was scanned for spilled food and feces (the majority of feces will be present in the 1.25-mm sieve). If applicable, food and feces were picked with tweezers and collected for weighing and determination of energy content by bomb calorimetry. Food intake (in grams) during the indirect calorimetry sessions was corrected for the amount of collected food spillage (in grams).

#### Determination of Energy Content of Food and Feces by Bomb Calorimetry

The energy content of the diets and the fecal pellets collected during indirect calorimetry was determined with an isoperibolic bomb calorimeter (Model Nr. 6400, Parr Instrument Company, IL). Energy content of the diets was



determined on food samples collected at different time points during the experiment (CD  $n = 9$ , HFD  $n = 10$ ). Energy intake was calculated by multiplying the mean energy content of the diets (kJ/g) with the amount of food intake (in grams).

The collected feces was weighed and grinded with metal balls for 2.5 min at 30 Hz (Tissue Lyser II, Retsch GmbH, Haan, Germany). Grinded feces was pressed into a pellet, weighed, and subjected to bomb calorimetry. Benzoic acid (~0.7 g) was added as combustion aid. Energy lost via feces was calculated for each mouse by multiplying the total amount of feces collected (in grams, see 2.4) by the energy content (kJ/g) determined by bomb calorimetry.

### Thermal Imaging

Thermal imaging was performed, as described previously (41), with 1- to 3-day-old newborn pups. In brief, at least three serial pictures were taken of each litter in six-well cell culture plates (T890 thermal imager, Testo, Lenzkirch, Germany). Image analysis was performed with the IRTSoft Software (version 4.6, Testo, Lenzkirch, Germany) and the temperature above the interscapular BAT depot (interscapular skin surface temperature, iSST) was determined.

### Genotyping

Genotyping was performed on earpieces obtained during tagging of the animals. Tissues were lysed (10 mM TRIS, 50 mM KCl, 0.45% Nonidet P40, 0.45% Tween-20, 10% gelatin in H<sub>2</sub>O at pH 8.3 with 0.2 mg/mL Proteinase K) for 4 h at 65°C and vigorous shaking. Proteinase K was inactivated by heating for 10 min at 95°C. PCR (denaturation: 5 min/95°C followed by 39 amplification cycles with 30 s/95°C, 45 s/54°C, 45 s/72°C, and a final elongation 10 min/72°C) was performed with three primers (Fig. 1A, “a”: AAGGCGCATA-ACGATACCAC, “b”: TACAATGCAGGCTCCAAACAC, “c”: CG-AGCACAGGAAGTTCAACA, Eurofins Genomics, Ebersberg, Germany) and the ImmoMix kit (Bioline, Cat. No. BIO-25020), according to the manufacturer’s instructions.

### RNA Isolation and cDNA Synthesis and Sequencing

RNA isolation was performed with TRIsure (Bioline, London, UK), following to the manufacturer’s instructions, from deep-frozen iBAT. Precipitated RNA was loaded to spin columns (SV Total RNA Isolation System, Promega, Cat. No. Z3105), centrifuged for 1 min with 12,000 g, and further processed according to the supplier’s instructions. RNA concentration was determined spectrophotometrically (Infinite 200 PRO NanoQuant, Tecan). cDNA synthesis was performed with 1 µg RNA (SensiFAST cDNA Synthesis Kit, Bioline, Cat. No. BIO-65053), according to the manufacturer’s instructions. PCR (denaturation: 10 min/95°C followed by 30 amplification cycles with 1 min/95°C, 30 s/54°C, 40 s/72°C, and a final elongation 5 min/72°C) was performed with primers (“d”: cggagtttcagcttgctggca, “e”: tcgcacagcttggtacgcttg, Eurofins Genomics, Ebersberg, Germany, Fig. 1A) and products were separated by gel electrophoresis on a 1% agarose gel. Separated PCR products were visualized under a UV light, cut, immediately weighed and stored at –20°C. PCR products were purified with the Wizard SV Genomic DNA Purification System (Promega, Cat. No.

A2361) and sent in to a commercial sequencing platform (Eurofins Genomics, Ebersberg, Germany). Analysis of sequencing results was performed with the “Benchling” platform (<https://www.benchling.com/>).

### Protein Expression Analysis by SDS-PAGE and Western Blot

Protein was isolated from interscapular BAT, homogenized in 10 µL/mg isolation buffer (50 mM Tris, 1% NP-40, 0.25% sodium deoxycholate, 150 mM NaCl, 1 mM EDTA) containing 0.1% phosphatase (Sigma-Aldrich, St. Louis, MO) and 0.1% protease inhibitor cocktail (Sigma-Aldrich, St. Louis MO), with a dispersing device (Micra D-1, Micra GmbH, Heitersheim, Germany). The homogenized samples were centrifuged 15 min at 4°C with 14,000 rcf. The clear layer of the supernatant was isolated by pipetting and centrifuged again. Samples were cleared from residual fat by a second extraction of the clear phase with a syringe. Protein concentrations were determined with the Pierce BCA Protein Assay Kit (Thermo Fisher Scientific, Rockford, IL), according to the manufacturer’s instructions. For protein detection, 30 µg protein were separated in a 12.5% SDS-PAGE and transferred to a nitrocellulose membrane. Subsequently, primary antibody was applied to detect UCP1 (ab23841, Abcam, UK, 1:5,000) followed by primary antibody detection using an IR-dye conjugated secondary antibody (IRDye 800CW, LI-COR, Lincoln, NE, 1:20,000). The IR signal was detected with the Azure Sapphire biomolecular imager (Azure Biosystems, Dublin, CA). Image analysis was conducted with the Image Studio Lite software version 5.2.

### DNA Extraction and 16S rRNA Sequencing

Cecal contents were collected together with other tissues and immediately snap frozen in liquid nitrogen and stored at –80°C. DNA isolation, library preparation, and sequencing were performed at the ZIEL – Core Facility Microbiome of the Technical University of Munich. Briefly, DNA was extracted using previously published protocols (44). For the assessment of bacterial communities, primers specifically targeting the V3–V4 region of the bacterial 16S rRNA {Forward-Primer [341 F- CCTACGGGNGGCWGCAG; Reverse-Primer (785r-ovh): GACTACHVGGGTATCTAATCC]} gene including a forward and reverse illumina-specific overhang and a barcode were used. Sequencing was performed using an Illumina MiSeq DNA platform. Obtained multiplexed sequencing files were analyzed using the IMNGS platform, which is based on the UPARSE approach for sequence quality check, chimera filtering, and cluster formation (45, 46). For the analysis, standard values for barcode mismatches, trimming, expected errors, and abundance cutoff were used and only sequences between 300 and 600 bp considered for analysis. Downstream analysis of the IMNGS platform output files were performed using the RHEA R pipeline (47). In brief, obtained abundances were normalized and quality of obtained sequences was assessed using rarefaction curves (48). Analysis of  $\alpha$ -diversity,  $\beta$ -diversity, and group comparisons were performed using default settings. Exceptions were applied for group comparisons for zOTUs and taxonomic levels (abundance cutoff 0.5 and exclusion of  $\alpha$ -diversity measures). Graphical output was modified for presentation using

inkscape (<https://inkscape.org>). Assignment of zOTUs to taxons was performed using the SILVA database (version 138.1 (49)). Assignment of species to specific zOTUs with EZBioCloud (50).

### Lipid Extraction and Mass Spectrometry Analysis

Lipid extraction for quantitative analysis using Lipidizer platform (SCIEX) was done using an adapted Methyl-tert-butyl-ether (MTBE) extraction protocol. Lipidizer internal standards mixture was prepared according to the manufacturer's instruction but dissolved in MTBE. To each 50  $\mu$ L plasma aliquot, 50  $\mu$ L water, 50  $\mu$ L internal standard, 500  $\mu$ L MTBE, and 160  $\mu$ L methanol were added, shortly vortexed and incubated on a mixer for 30 min. Water (200  $\mu$ L) was added and centrifuged at 16,000 g. The supernatant was transferred in vials and the residual phase reextracted using MTBE:methanol:water in the ratio 3:1:1. The collected supernatants were evaporated with a vacuum centrifuge and resuspended in 250  $\mu$ L of 10 mM ammonium acetate in dichloromethane:methanol [50:50 (vol/vol)].

Samples were analyzed using a QTRAP 5500 (AB SCIEX) equipped with differential mobility spectrometer (DMS) interface (51) operating with SelexION technology, coupled to a Shimadzu Nexera X2 liquid chromatography system. The Lipidizer platform was operated via the software Analyst version 1.6.8 and Lipidomics workflow manager (SCIEX). A detailed description of this shotgun approach has been previously reported (52). The Lipidizer Platform was tuned using the SelexION Tuning Kit (SCIEX), according to the manufacturer's recommendations, and a system suitability test was performed using the System Suitability Kit (SCIEX), according to the manufacturer's instructions. The Lipidizer Platform uses 10 mM ammonium acetate in dichloromethane: methanol [50:50 (vol/vol)] as running buffer, dichloromethane: methanol [50:50 (vol/vol)] as rinse 0&1, 2-propanol as rinses 2&3, and 1-propanol as a DMS modifier. Samples (50  $\mu$ L) were injected for each of the two MRM methods: one with a DMS on and one with DMS off. MRM data acquisition, processing, and quantification was performed automatically by the lipidizer lipidomics workflow manager. Lipid concentrations are given in nmol/mL.

### Data Analysis and Statistics

General data analysis was performed with R (version 4.0.3) within R-Studio (version 1.3.1093). Unless otherwise indicated data are represented as means  $\pm$  SD or with single values for each mouse. Student's *t* tests were performed with the package "ggpubr" (version 0.4.0). ANOVA and linear model analysis with the package "stats" (version 4.0.3). Trapezoid area under the curves were calculated using the AUC function of the package "DescTools" (version 0.99.38).

Analysis of  $\alpha$ -diversity was performed with Prism 6 (GraphPad Software Inc., La Jolla, CA) using nonparametric Mann-Whitney *U* test.  $\beta$ -Diversity is visualized using nonmetric multidimensional scaling based on generalized UniFrac and tested for significance using PERMANOVA. Differences in zOTUs have been determined using Kruskal-Wallis rank sum test with adjustments for multiple testing using the Benjamini & Hochberg method.

Multimomics analysis was performed using R (version 4.0.4) and python (version 3.8.5). Multimomics factor analysis (MOFA) (53, 54) was used for unsupervised data integration of the lipidome and microbiome data. The mofapy2 python package (version 0.5.8) and the MOFA2 R package (version 1.0.1) (for downstream analysis) were used together with custom visualization tools. Data integration analysis for 'omics studies (DIABLO) (55) was used as a supervised analysis framework. DIABLO generalizes (sparse) partial least-squares discriminant analysis (PLS-DA) for the integration of multiple data sets measured on the same samples. For DIABLO analyses, the mixOmics R package (version 6.14.0) (56) was used along with custom code for randomized performance estimation.

## RESULTS

### Deletion of UCP1 Exon 2 Leads to a Loss of Protein Expression

The original mouse used to generate the knockout of UCP1 in the mice used in this study was generated in frame of the EUCOMM program via a "knockout first allele" approach (39, 40). The *lacZ* and the *neo* resistance cassette were removed from the UCP1<sup>tm1a</sup> allele, by crossbreeding with flippase-expressing mice (Fig. 1A1), thus generating WT (UCP1<sup>tm1c</sup>) mice. These mice containing only one flippase recognition target (*FRT*) and two *loxP* sites flanking exon 2 of the *Ucp1* gene were crossed with mice expressing Cre-recombinase under the control of the *Rosa26* promoter (*Rosa26Cre/+*) (Fig. 1A2). This resulted in the generation of KO (UCP1<sup>tm1d</sup>) mice by constitutive germline deletion of exon 2 in the *Ucp1* gene (Fig. 1A3). Deletion of exon 2 was first confirmed by PCR on genomic DNA with one forward and two reverse primers binding to distinct sites of the *Ucp1* gene (Fig. 1, A2 and A3). As predicted, this resulted in a short (263 bp) product for WT mice (Fig. 1B, primers a–b) and a longer (388 bp) product for KO (Fig. 1B, primers a–c), whereas HET mice showed both products. Of note, the 1,255 bp product generated by the primers a and c in WT and HET is not seen, as the elongation period of the PCR protocol is too short to produce a product of this size. To further investigate the consequences of exon 2 deletion, we performed a RT-PCR on RNA isolated from brown adipose tissue of both WT and KO mice. For the primer pair binding in exon 1 (d) and exon 5 (e) of the *Ucp1* gene (Fig. 1A), KO showed a smaller product size (~500 bp) compared with WT mice (~700 bp), as predicted by in-silico PCR (KO: 508 bp, WT: 707 bp, <https://genome.ucsc.edu/cgi-bin/hgPcr>) (Fig. 1C). Subsequent sequencing of the WT and KO PCR products revealed that the deletion of exon 2 causes a frame shift, leading to a premature stop codon in exon 3 (Supplemental Fig. S1; see <https://doi.org/10.6084/m9.figshare.15112227>). Consequently, KO mice do not express UCP1 protein, as confirmed by Western blot analysis (Fig. 1D, Supplemental Fig. S2; see <https://doi.org/10.6084/m9.figshare.15112233>).

### Thermogenic Deficiency Leads to Decreased Body Weight in Young KO Mice

The loss of the major protein responsible for nonshivering thermogenesis resulted in a clear reduction of interscapular

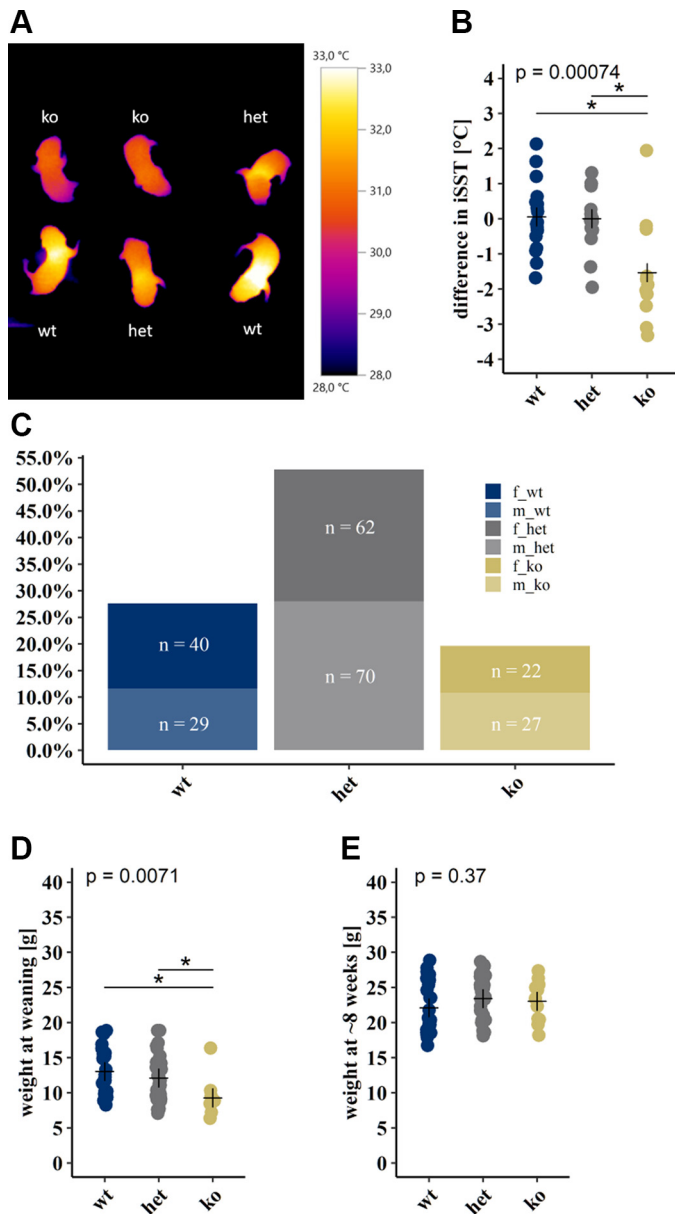


**Figure 2.** Lack of *Ucp1* leads to phenotypic alterations in young mice. **A:** representative thermal image of newborn pups (2–3 days) of a *Ucp1*-HET breeding pair. **B:** analysis of interscapular skin surface temperature [iSST,  $n(\text{wt}) = 17$ ,  $n(\text{het}) = 17$ ,  $n(\text{ko}) = 11$ ,  $N = 45$  of 5 litters]. **C:** offspring genotype distribution of *Ucp1*-HET breeding pairs ( $n = 15$ ) ( $N = 250$ ). Body weight of female and male *Ucp1*-WT ( $n = 23$ ), *Ucp1*-HET ( $n = 33$ ), and *Ucp1*-KO ( $n = 11$ ) mice (**D**) at weaning and at the age of 8 wk ( $N = 67$  of 9 litters) (**E**). **A–E:** all mice were bred and housed at 23°C ambient temperature. **B, D, and E:** crosses indicating group means. One-way ANOVA and *t* test with Bonferroni adjusted *P* value, \**P* value < 0.05.

skin surface temperature (iSST) in newborn KO compared with WT mice (Fig. 2, **A** and **B**). The loss of one functional *Ucp1* allele on the other hand had no implication on iSST in newborn HET pups compared with WT pups (Fig. 2, **A** and **B**). The genotype distribution of offspring from HET/HET breeding pairs (generation F2–F3) did not significantly deviate from the Mendelian distribution of 1:2:1 (Fig. 2C and Table 2). However, KO mice had lower body weight at weaning (at the age of ~3–4 wk) compared with HET and WT

mice (Fig. 2D), a phenotype that could be confirmed in the conventional UCP1-KO mouse on 129S1/SvImJ; a similar trend was also observed in the conventional UCP1-KO on C57Bl/6J (Supplemental Fig. S3, **A** and **C**; see <https://doi.org/10.6084/m9.figshare.15112236>). Irrespective of the knockout model, body weight of all three genotypes were similar at ~8 wk of age (Fig. 2E, Supplemental Fig. S3, **B** and **D**).

In summary, this suggests a strain-dependent effect of UCP1 ablation on early body weight that recovers with age.

### UCP1-KO and WT Mice Have Similar Susceptibility to DIO at Thermoneutrality

The susceptibility of UCP1-KO mice to diet-induced obesity (DIO) under thermoneutral conditions is still a matter of debate. We addressed this controversial question using our novel UCP1-KO model by feeding mice at thermoneutrality a control diet (CD) for 4 wk followed by 8 wk of high-fat diet (HFD). At the start of the experiment, at the age of 8 wk, mice of both genotypes had similar body weights (data not shown). Cumulative body weight gain increased with time but was similar between both genotypes (Fig. 3A), as indicated by linear model analysis during CD (Duration  $P < 0.001$ , Genotype  $P = 0.491$ ) and HFD (Duration  $P < 0.001$ , Genotype  $P = 0.188$ ) feeding. In line, total energy intake between both genotypes was similar during control diet (CD) and high-fat diet (HFD) feeding (Fig. 3, **B** and **C**).

We determined body composition in terms of lean and fat mass at different time points of the experiment. Both lean mass (Fig. 3D) and fat mass (Fig. 3E) correlated well with body weight during both feeding regimes, with fat mass being the main contributor to the increase in body weight during HFD feeding ( $R^2 > 0.9$ ), in both WT and KO mice (Fig. 3, **D** and **E**).

UCP1 knockout mice have been described to be metabolically more efficient (29, 31, 32), thus incorporating more fat mass per unit of energy intake. We addressed this question by linear model analysis of cumulative fat mass gain versus cumulative energy intake over the experimental period (Fig. 3F). There was no difference in the correlation of fat mass gain and energy intake between genotypes, consequently both UCP1-WT and UCP1-KO mice showed similar metabolic efficiency. Of note, this result was confirmed by determining metabolic efficacy as the percentage of food energy stored as fat mass, as described previously (31) (Supplemental Fig. S4, **A** and **B**; see <https://doi.org/10.6084/m9.figshare.17088992>). The similarity in fat mass of both UCP1-WT and UCP1-KO determined by NMR was reinforced by dissected weights of iWAT, eWAT, and iBAT (Fig. 3, **G–I**). Collectively, these data analyses demonstrate that UCP1 ablation neither affected energy intake, nor body adiposity, nor metabolic efficacy when mice were kept at thermoneutral conditions.

**Table 2.** Offspring genotype distribution of heterozygous breeding pairs

Genotype	<i>n</i>	Observed, %	Expected, %	<i>P</i> ( $\chi^2$ Test)
UCP1-WT	69	27.6	25	0.1364
UCP1-HET	132	52.8	50	
UCP1-KO	49	19.6	25	

KO, knockout; WT, wild type.



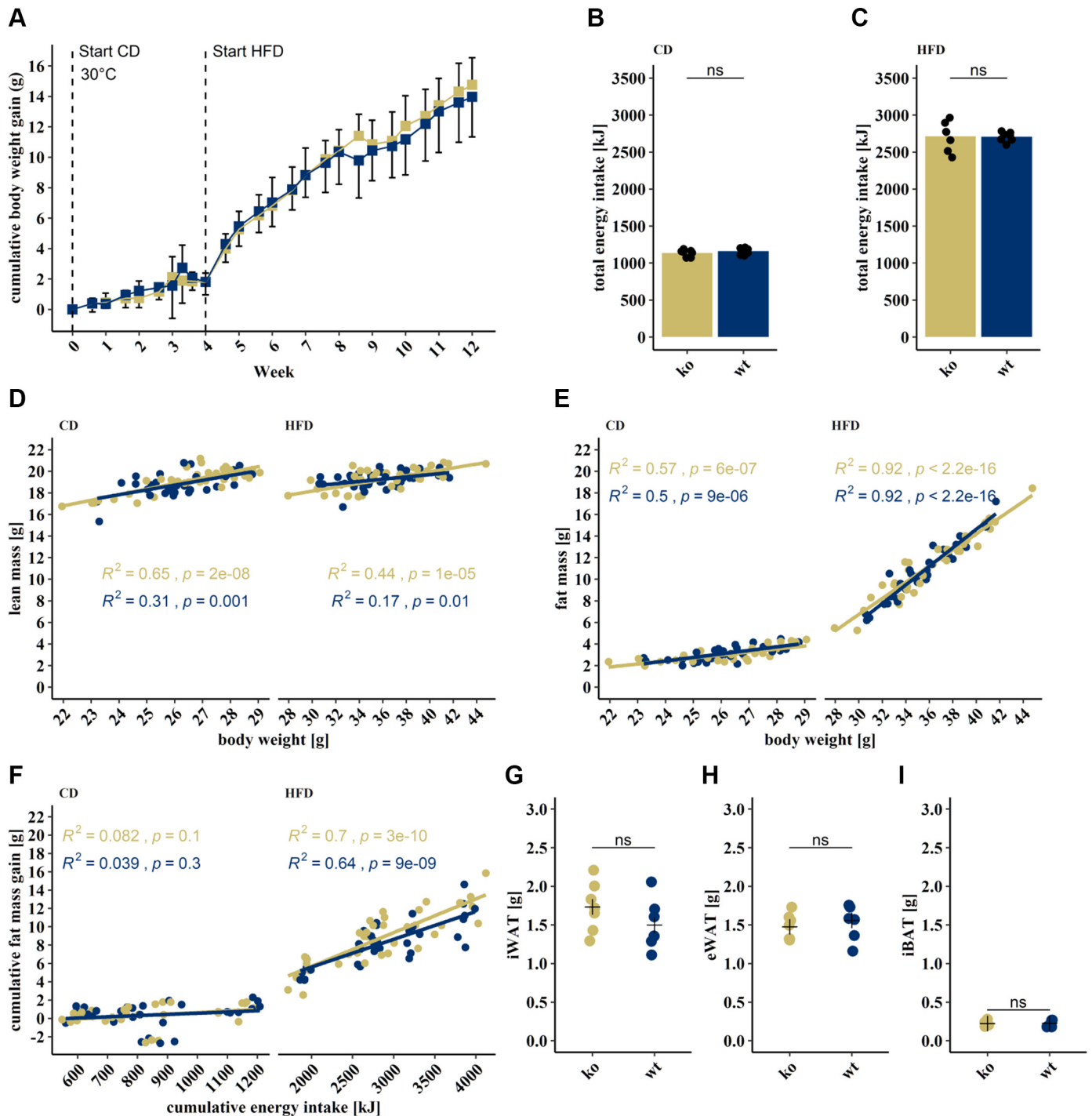


**Figure 3.** Similar susceptibility to diet-induced obesity in UCP1-KO and wild-type (WT) mice. **A:** body weight of Ucp1-WT (wt,  $n = 7$ ) and Ucp1-KO (ko,  $n = 7$ ) mice at 30°C fed a control (CD) or high-fat diet (HFD). Total energy intake of mice during CD (**B**) and HFD (**C**) feeding. Pearson correlation coefficient between measurements of lean mass and body weight (**D**) and fat mass and body weight (**E**) during CD (left) and HFD (right) feeding. **F:** metabolic efficiency in terms of correlation (Pearson's correlation coefficient) between cumulative fat mass gain and cumulative energy intake for CD (left) and HFD (right). Weights of dissected inguinal white adipose tissue (iWAT; **G**), epididymal white adipose tissue (eWAT; **H**), and interscapular brown adipose tissue (iBAT; **I**) at the end of HFD feeding. Student's  $t$  test ns =  $P$  value  $> 0.05$ . Group means indicated as bars (**B** and **C**) and crosses (**G–I**). KO, knockout.

### Plasma Lipid Composition of UCP1-KO and UCP1-WT Mice Is Comparable

Activated BAT can clear substantial amounts of lipids from circulation (2, 57). To study whether UCP1 ablation

affected systemic lipid metabolism, a targeted lipidomic approach on plasma samples was performed. Lipid class composition was similar between both genotypes. Only cholesteryl esters (CE) were significantly more abundant in UCP1-WT compared with UCP1-KO mice (Fig. 4A). Concen-



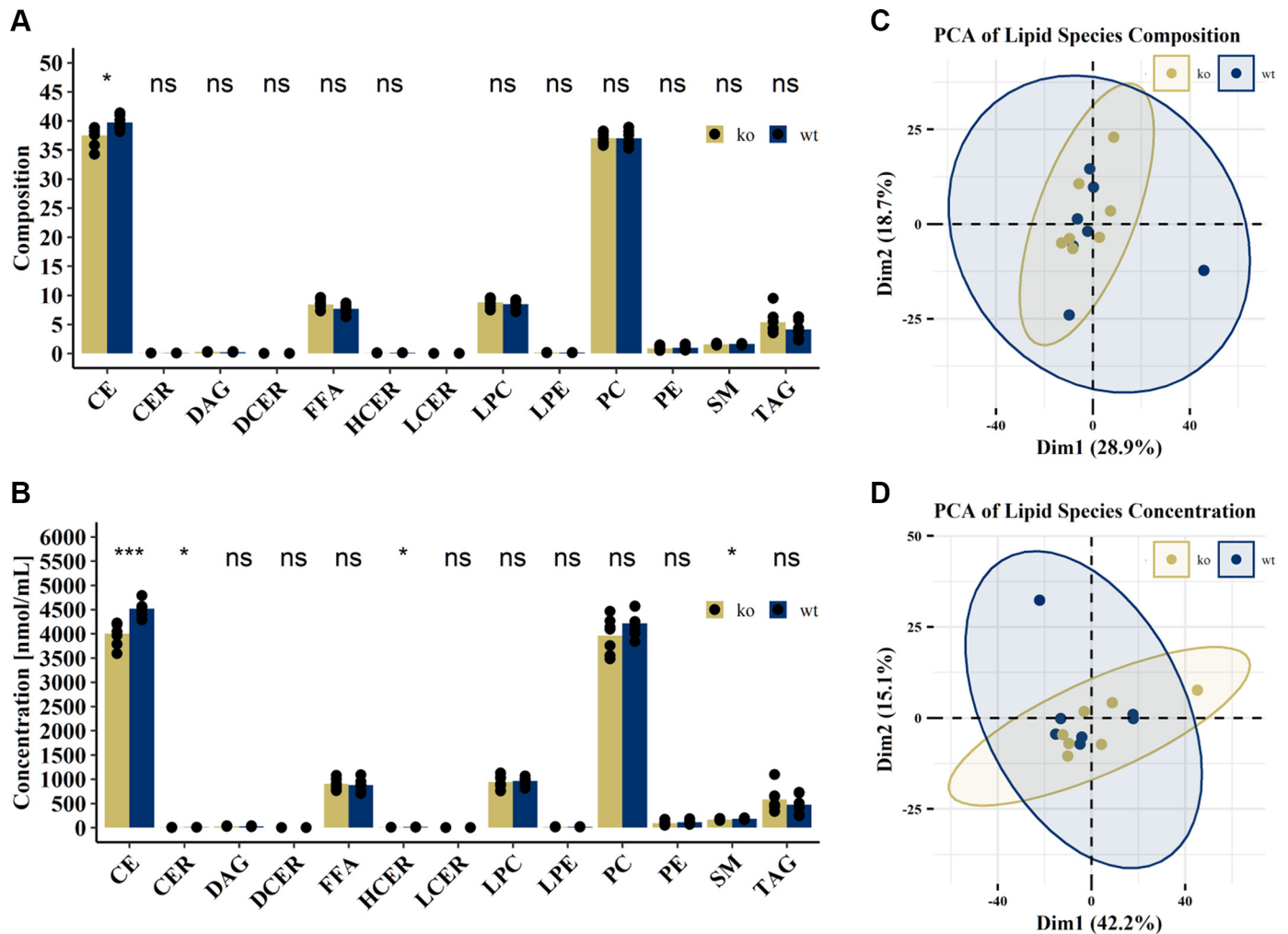


**Figure 4.** Plasma lipid profiles are comparable between UCP1-KO and UCP1-WT. Composition (A) and concentration (B) of lipid classes in plasma of UCP1-KO (ko,  $n = 7$ ) and UCP1-WT (wt,  $n = 7$ ) mice housed at 30°C after 8 wk of high-fat diet feeding. Principal component analysis (PCA) of lipid species composition (C) and concentration (D). A and B: Student's  $t$  test ns =  $P$  value  $> 0.05$ , \* $P$  value  $< 0.05$ , \*\*\* $P$  value  $< 0.001$ . Group means indicated as bars (A and B). CE, cholesteryl esters; CER, ceramides; DAG, diacylglycerols; DCER, dihydroceramides; FFA, free fatty acids; HCER, hexosylceramides; KO, knockout; CER, lactosylceramides; LPC, lysophosphatidylcholines; LPE, lysophosphatidylethanolamines; PC, phosphatidylcholines; PE, phosphatidylethanolamines; SM, sphingomyelins; TAG, triacylglycerols; WT, wild type.

Concentrations of CE, ceramides (CER), hexosylceramides (HCER), and sphingomyelins (SM) were significantly higher in UCP1-WT mice (Fig. 4B). However, fold changes (FC) between two UCP1-KO were rather small (CE,  $FC_{wt/ko} = 1.13$ ; CER,  $FC_{wt/ko} = 1.17$ ; HCER  $FC_{wt/ko} = 1.16$ ; SM,  $FC_{wt/ko} = 1.1$ ). The similarity of plasma lipid composition between both genotypes was confirmed by principal component analysis (PCA) of composition (Fig. 4C) and concentration (Fig. 4D) on a lipid species level.

Collectively, these data demonstrate that ablation of UCP1 did have only minor effects on steady-state systemic lipid metabolism at thermoneutrality.

#### Lack of UCP1 Is Associated with the Abundance of Specific Microbial Genera

The gut microbiome influences host metabolism (19) and studies report effects of microbiome composition on UCP1 expression (21) and thermogenesis (20). As an alternative host-driven approach, we investigated whether the absence

of UCP1 alters microbiome composition, by comparing the cecal microbiomes of UCP1-WT and UCP1-KO mice. Similar bacterial richness ( $\alpha$ -diversity) was observed between genotypes by 16S rRNA analysis (Fig. 5A). However, ablation of UCP1 affected cecal microbial composition demonstrated by differences in  $\beta$ -diversity between genotypes (Fig. 5B). Detailed analysis of the microbial composition revealed four zOTU significantly different between UCP1-KO and UCP1-WT based on unadjusted Kruskal-Wallis rank sum test (Fig. 5, C–F). After adjustment for multiple comparisons, two of these zOTUs demonstrated a trend to higher abundance in UCP1-KO, whereas two others were significantly more abundant in UCP1-WT mice. These zOTUs could be assigned to *Parabacteroides goldsteinii* (zOTU3 and zOTU4) and *Desulfovibrio fairfieldensis* (zOTU17 and zOTU19), respectively.

The microbiome can substantially influence host lipid metabolism (58). As we identified small changes in both lipid metabolism and microbiome composition, we investigated potential interactions between microbiome and lipidome.

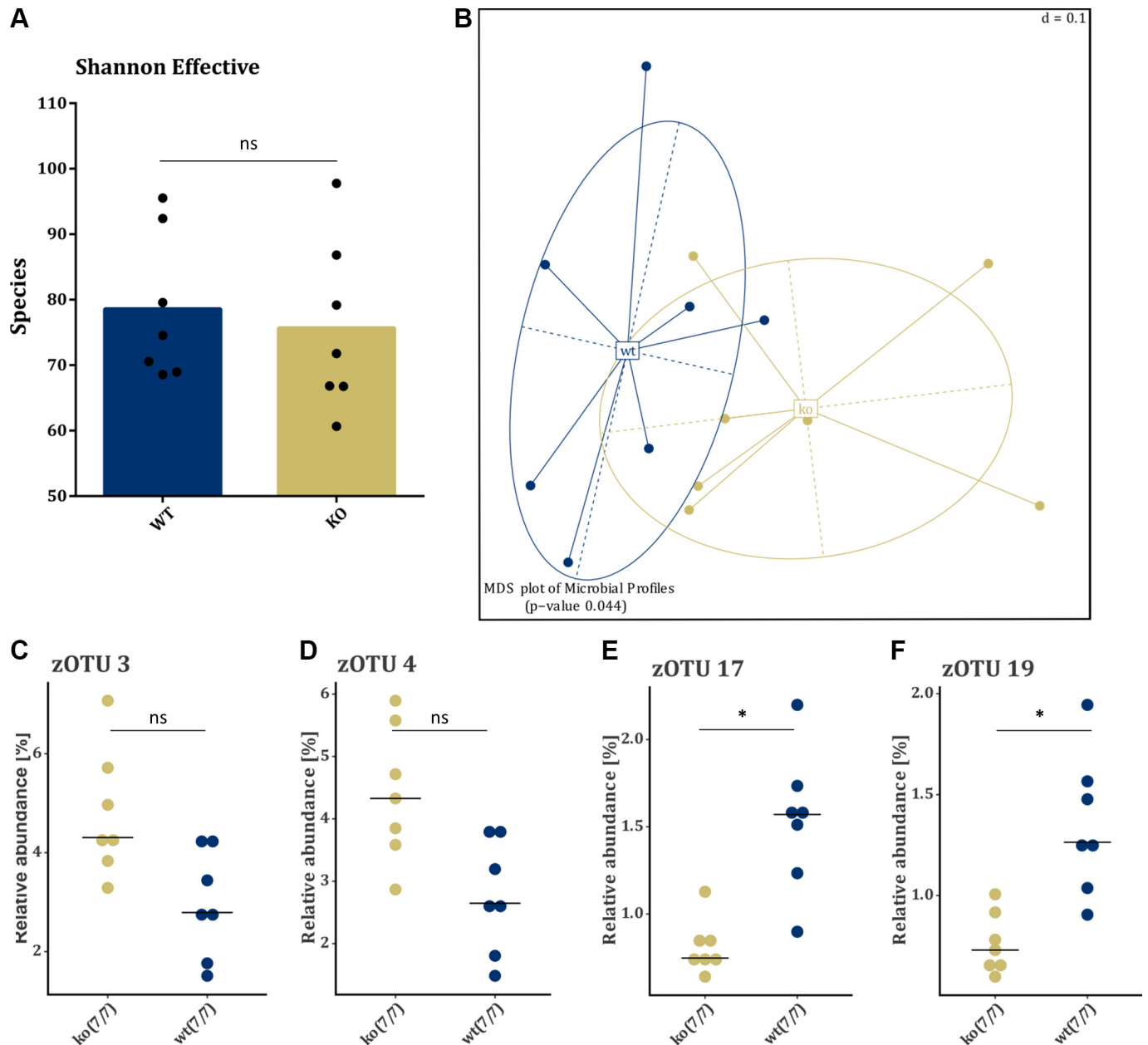


**Figure 5.** Single cecal microbial genera are associated with the presence of UCP1. Analysis of cecal microbiome of UCP1-KO (ko,  $n = 7$ ) and UCP1-WT (wt,  $n = 7$ ) mice housed at 30°C after 8 wk of high-fat diet feeding. Comparison of  $\alpha$ -diversity determined by Shannon effective index (A) and  $\beta$ -diversity assessed by principal coordinates analysis (B). C–F: relative abundance of zOTU identified by statistically different unadjusted Kruskal–Wallis rank-sum test between WT and KO mice. Statistical differences tested by nonparametric Mann–Whitney  $U$  test (A) ns =  $P$  value  $> 0.05$ , permutational multivariate analysis of variance (B), Kruskal–Wallis rank-sum test with the Benjamini & Hochberg adjustment (C–F). ns =  $P$  value  $> 0.05$ , \* $P$  value  $< 0.05$ , Group means indicated as bars (A) and lines (C–F). KO, knockout; WT, wild type.

Therefore, we analyzed the combined lipidome and microbiome data set using supervised (DIABLO PLS-DA) and unsupervised (MOFA) approaches. DIABLO PLS-DA revealed two sets of features that discriminated between UCP1-KO and UCP1-WT mice (Fig. 6A). However, quality assessment by repeated analysis of the data set with randomly assigned groups (1,000 iterations) demonstrated similar good discrimination as between UCP1-KO and UCP1-WT mice (Fig. 6A). Consequently, it was not possible to discriminate the observed difference between UCP1-KO and UCP1-WT from random differences between samples. This assumption was

confirmed by unsupervised MOFA demonstrating no separation of the two genotypes by the two factor groups explaining the highest proportion of variance between UCP1-KO and UCP1-WT mice (Fig. 6B).

Consequently, no genotype specific interactions between plasma lipid composition and the microbiome were identified.

#### UCP1-KO Mice Have Similar Energy Balance at Thermoneutrality

The effect of UCP1 knockout on energy balance regulation was investigated in detail by indirect calorimetry

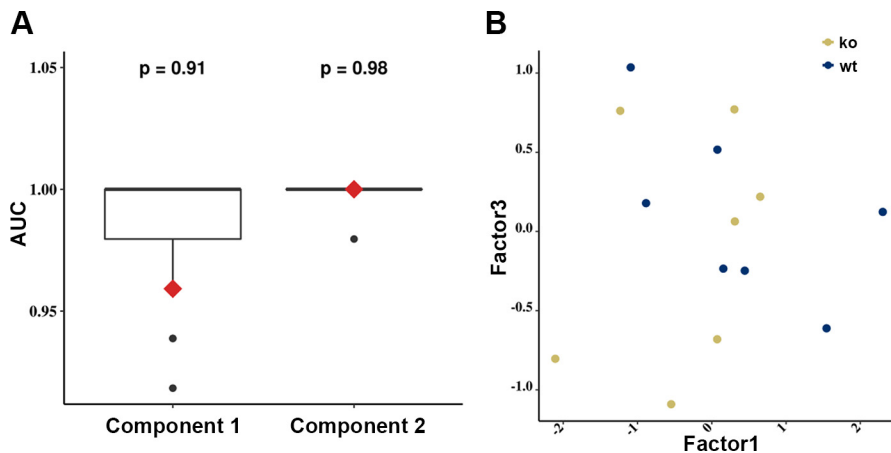


**Figure 6.** Multiomics reveal no interaction between microbiome and lipidome explaining differences between UCP1-KO and UCP1-WT mice. Integrated analysis of the combined lipidome and microbiome data sets. A: receiver operating characteristic area under the curve (AUC) of data integration analysis for biomarker discovery using a latent components partial least squares discriminant analysis (DIABLO PLS-DA). Red diamonds indicate results of supervised DIABLO PLSA-DA of the components 1 and 2 (Comp1, Comp2). Box plots indicate results of 1,000 randomized DIABLO PLS-DA analyses.  $P$  value =  $\#(\text{AUC}_{\text{sup}} < \text{AUC}_{\text{ran}})/1,000$ . B: visualization of the two factors explaining most of the variance between UCP1-KO and UCP1-WT mice based on multiomics factor analysis (MOFA). KO, knockout; WT, wild type.

measurements 3–4 wk after the start of CD or HFD feeding. We observed a clear diurnal pattern of the respiratory exchange ratio during CD feeding, being higher during the dark phase compared with the light phase (Fig. 7, A and B) indicating that mice utilized more carbohydrates during the nocturnal activity phase while relying more on fatty acid metabolism during the daytime resting phase. During HFD feeding, the respiratory exchange ratio was generally reduced compared with the CD period, demonstrating a shift in substrate utilization toward fatty acid oxidation based in the high-fat content of the diet (Fig. 7, C and D). However, no differences in respiratory exchange ratio between KO and WT mice were detected during either feeding period (Fig. 7, B and D).

Enhanced recurrent activation of BAT thermogenesis by meal-associated thermogenesis and/or chronic BAT activation for diet-induced thermogenesis might both contribute to total energy expenditure and thus protect WT mice from diet-induced obesity (31). To scrutinize these findings, we investigated whether knockout of UCP1 affected energy expenditure in the new mouse model. As expected, metabolic rate in terms of  $\text{O}_2$  consumption,  $\text{CO}_2$  production and heat production were subject to diurnal alterations during CD and HFD feeding, increasing during the nocturnal activity phase, and decreasing during the daytime resting phase (Fig. 7, E and G and Supplemental Fig. S5, A–F; see <https://doi.org/10.6084/m9.figshare.15112245>). However, energy expenditure (area under the heat production curve) during the measurements were similar between WT and KO mice at all times (Fig. 7, F and H and Supplemental Fig. S5, E and F). Consequently, knockout of UCP1 did not affect energy expenditure at thermoneutral conditions.

Subsequent to the energy expenditure measurement during HFD feeding, we investigated basal metabolic rate and noradrenaline (NA)-induced heat production in fasted mice. KO and WT mice had similar basal metabolic rate (Fig. 7I) and increased metabolic rates after NA injection, similar to previous observations (59, 60). However, WT showed a remarkably higher response upon NA injection compared with KO (Fig. 7, J–L), demonstrating the capacity for UCP1-mediated thermogenesis.

In addition to energy expenditure, we measured energy intake and fecal energy excretion during the calorimetry

sessions. Fecal energy content was higher during high-fat diet compared with control diet feeding, reflecting the increased energy content of the high-fat diet (not shown). However, there was no difference between genotypes in either feeding period (Fig. 8, A and B). This was also found for excreted (Fig. 8, C and D) and ingested (Fig. 8, E and F) energy during the calorimetry sessions. Consequently, energy balance was unaffected by the ablation of UCP1 under thermoneutral conditions (Supplemental Fig. S4, C and D). Regarding these energy balance data, we observed a high surplus of energy over a measuring period of 3 days during CD and 4 days during HFD feeding. Of note, the measuring periods of energy intake and energy excretion via feces (3 days CD and 4 days HFD) compared with energy expenditure (2 days CD, 3 days HFD) differed by ~1 day due to technical issues with the calorimetry device. We aimed to correct this by imputation of the missing energy expenditure data. Therefore, for each mouse hourly mean energy expenditure values were calculated separately for the dark and light phase from the existing data. These values were then multiplied by the amount of missing hours for each phase. These corrections resulted in a reduction of the daily energy surplus to an average of 18.5 kJ/day (CD) and 19 kJ/day (HFD). However, the conclusion that energy balance was unaffected by the deletion of UCP1 under thermoneutral conditions was unchanged, as no differences between genotypes were detected (Fig. 8, G and H).

## DISCUSSION

We characterize a novel UCP1 knockout model, as an alternative to the established and widely used UCP1-KO mouse, generated by Leslie Kozak and coworkers (26). In regard of the conflicting data published so far on the DIO susceptibility of this established UCP1-KO model, there is an urgent need for new models generated by cutting edge transgenic technologies to enable robust validation of metabolic functions for UCP1. Comprehensive metabolic phenotyping of the novel UCP1-KO mouse model presented in this study will help to clarify the role of UCP1 in brown and brite/beige adipose tissues for energy balance regulation, contrasting diet- and cold-induced nonshivering thermogenesis. Down this line, another UCP1-KO mouse model lacking functional



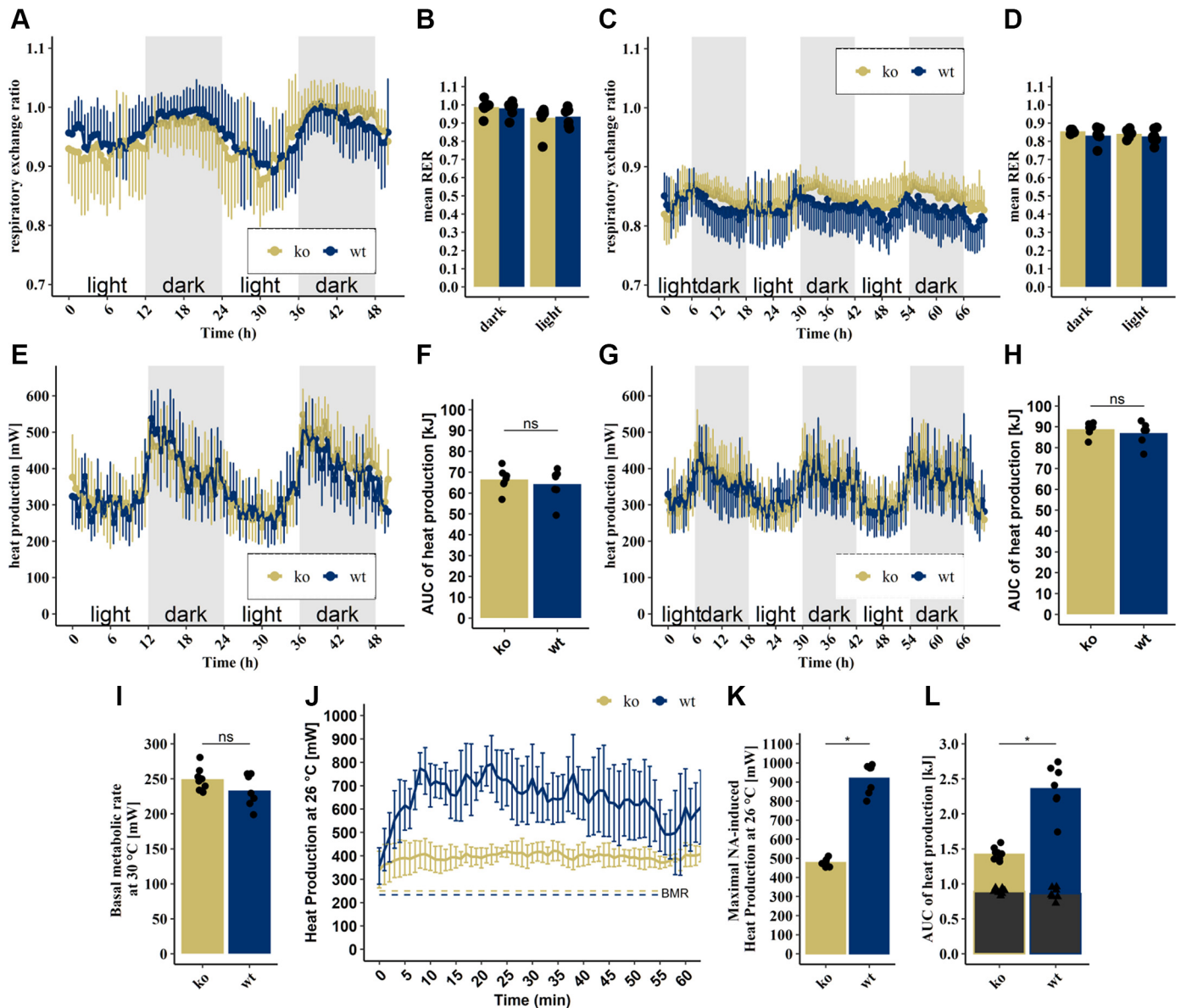


**Figure 7.** Energy expenditure at thermoneutrality is comparable between Ucp1-KO (ko,  $n = 7$ ) and Ucp1-WT (wt,  $n = 7$ ) mice during CD feeding. **A:** respiratory exchange ratio of Ucp1-KO (ko,  $n = 7$ ) and Ucp1-WT (wt,  $n = 7$ ) mice during CD feeding. **B:** mean respiratory exchange ratio (RER) of dark and light phases corresponding to **A**. **C:** respiratory exchange ratio of mice during HFD feeding. **D:** mean respiratory exchange ratio (RER) of dark and light phases corresponding to **C**. **E:** Heat production during CD feeding (**E**) and the respective area under the curve (AUC; **F**). **G:** Heat production during HFD feeding (**G**) and the respective area under the curve (AUC; **H**). **I:** mean basal metabolic rate (mean of the four consecutive lowest values after at least 3 h of fasting) at 30°C. **J:** heat production curve of mice injected with noradrenalin at 26°C. Dashed lines indicate basal metabolic rate (BMR) measured at 30°C (**K**). Maximal heat production during the 80-min measurement interval shown in **J**. **L:** AUC of heat production corresponding to **J**. Gray bars and triangles indicating contribution of basal metabolic rate. Students  $t$  test,  $ns = P > 0.5$ ,  $*P < 0.05$ , bars indicate group means (**F**, **H**, **I**, **K**, and **L**); Data represented as means and standard deviation, averaged over a period of 30 min (**A**, **C**, **E**, and **G**); Data represented as means and standard deviation, averaged over a period of 10 min (**J**). CD, control diet; HFD, high-fat diet; KO, knockout; WT, wild type.

UCP1 due to a SNP at nucleotide 38 of exon 5 in the *Ucp1* gene will also be instrumental for comparative studies (15).

The aim of this study was to compare the metabolic phenotype of the new UCP1 knockout mouse with established UCP1-KO mouse models, especially in light of the still ongoing debate whether (29–33) or not (10, 17, 26–28) the UCP1 ablation renders mice more susceptible to DIO at thermoneutral conditions. Other than at thermoneutrality, mice at standard housing conditions (~23°C ambient temperature) must constitutively recruit substantial thermoregula-

tory heat production to maintain normothermia. Mice lacking UCP1 recruit other thermogenic mechanisms to defend body temperature at these conditions and in contrast to WT mice may be protected against DIO (16–18).

The ablation of UCP1 impaired BAT thermogenesis in newborns and in adult mice, as assessed by infrared thermography and indirect calorimetry, respectively. In line with a previous report (41), UCP1-KO pups showed decreased interscapular skin temperature (iSST) and decreased weight at the time of weaning, confirming the significance of UCP1

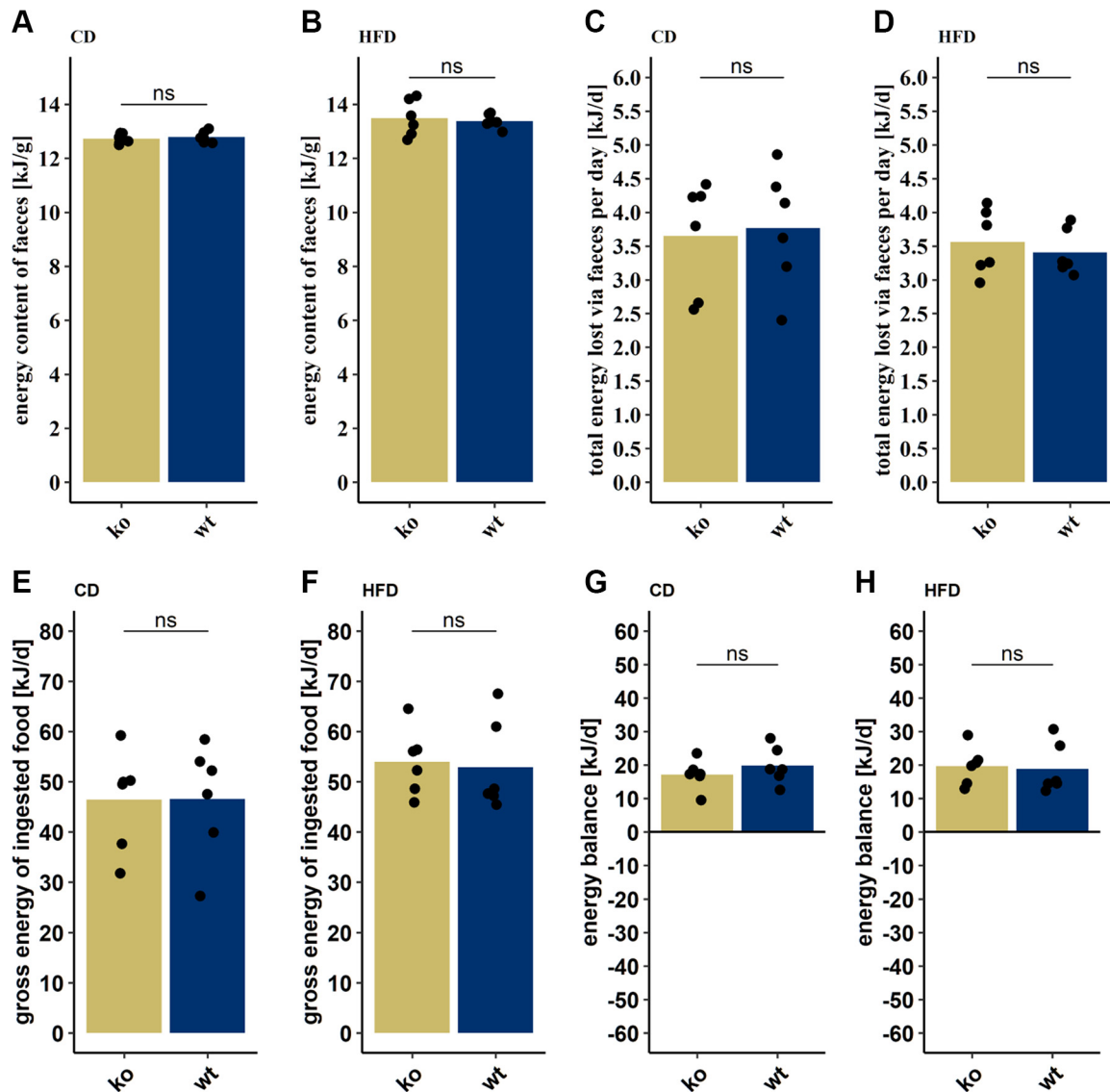


**Figure 8.** Knockout of *Ucp1* does not influence energy balance at thermoneutrality. Fecal energy content of *Ucp1*-WT ( $n = 6$ ) and *Ucp1*-KO ( $n = 6$ ) fed CD (A) or HFD (B). Total energy lost via feces of mice fed CD (C) or HFD (D). Energy consumption of mice fed CD (E) or HFD (F). Energy balance of mice during CD (G) or HFD (H) feeding. One mouse (wt) was removed, as it did not eat during the calorimetry session. Another one (ko) was removed from the analysis, as the fecal samples did not combust completely. Students *t* test, ns =  $P > 0.5$ , bars indicate group means. CD, control diet; HFD, high-fat diet; KO, knockout; WT, wild type.

as an efficient mechanism to defend body temperature in early life. In adult mice showing no difference in body mass or body composition, the capacity for norepinephrine-induced thermogenesis was strongly attenuated in UCP1 KO compared with WT mice. Thus, the lack of UCP1 in BAT results in a substantial deficiency in thermogenesis.

Once the need for active thermoregulatory, heat production is eliminated by housing mice in their thermoneutral zone (27°C–30°C) the effect of UCP1 deletion becomes inconclusive. It has been repeatedly demonstrated that high-fat diet feeding increases UCP1 gene expression in BAT at thermoneutrality, which is most likely due to the increased activity of the sympathetic nerves projecting into BAT. Eventually, the diet-induced release of norepinephrine from sympathetic varicosities in BAT would also stimulate UCP1-mediated thermogenesis, even at thermoneutral housing

temperature. Enforced dissipation of excess dietary calories as heat in BAT, if operating at an adequate rate, could thereby protect wild-type mice from excessive weight gain caused by overfeeding (61, 62). In this scenario, considering UCP1 as the main contributor to BAT thermogenesis, it seems plausible that body fat accretion should be accelerated in mice lacking UCP1 when fed a high-fat diet at thermoneutrality. Indeed, results from several studies concluded that UCP1-KO mice housed at thermoneutrality are more susceptible to DIO due to the lack of diet-induced thermogenesis in BAT (29–32).

We investigated this phenomenon by comprehensive metabolic analysis of the novel UCP1-KO model. Total energy expenditure was similar in both KO and WT mice and did not differ during the nocturnal feeding period, indicating no effect of UCP1 ablation on diet-induced thermogenesis.

Furthermore, considering the similarities in body weight gain, food intake, metabolic efficiency, and energy balance between KO and WT mice, there is no evidence for a more DIO-susceptible phenotype of UCP1-KO mice. These findings are in line with various studies on the established UCP1-KO mouse (10, 26–28) and a second recently described UCP1-KO mouse (15).

The lack of increased DIO susceptibility in UCP1-ablated mice is perhaps unexpected in the light of recent reports identifying the gut hormone secretin as the mediator of meal-associated thermogenesis in BAT and the role of secretin-induced BAT thermogenesis for satiation and meal termination. The effects of secretin on BAT thermogenesis, however, are transient and affect meal patterning, but do not reduce daily energy intake. Chronic infusion of a secretin analog in DIO mice transiently elevated energy expenditure, but did not reduce body adiposity. Reminiscent of leptin and ghrelin resistance, it may well be that DIO mice are also resistant to the thermogenic effects of secretin in BAT.

In regard of the conflicting results from different UCP1-KO models, it remains difficult to draw a firm conclusion on whether or not energy balance regulation and DIO are affected by the absence of UCP1 at thermoneutrality. We would like to emphasize, however, that we took particular care in our study to exclude possible pitfalls and adjust for confounding factors that may have contributed to diverging results of previous studies (see Table 1). First, the new UCP1 KO model was bred on the C57BL/6N background, a strain with higher DIO susceptibility than the widely used C57BL/6J strain. Second, we studied WT and KO mice derived from heterozygous breeding pairs thus enabling the inclusion of littermates. Thereby, gene drift known to occur in homozygous breeding schemes as well as cage effects and maternal effects potentially programming metabolism of offspring were controlled. Third, diets used in the present study were chemically defined to differ only in the macronutrient composition. Fourth, we monitored energy intake, fecal energy excretion, body composition, and energy expenditure, thus delivering a comprehensive assessment of energy balance and metabolic efficiency. Finally, we also addressed potential changes in gut microbiota composition, as accumulating evidence suggests that richness and diversity of bacteria in the gastrointestinal tract impact host metabolism. DIO susceptibility in UCP1-KO may be related to effects on host metabolism due to genotype-dependent alterations in gut microbiota. Interestingly, two zOTUs upregulated in UCP1-KO were assigned to *P. goldsteinii*. The abundance of this bacterial species has previously been reported to decrease in DIO and diabetes and to increase UCP1 expression in iBAT and iWAT of C57BL/6J mice (21). It seems worthwhile to further investigate the underlying nature of this interrelationship between *P. goldsteinii* and thermogenic adipose tissues. Possibly, differences in the gut microbiota ecosystems colonizing mice in different housing facilities are an underestimated factor, so far, contributing to diverging results reported in the literature.

For future studies, a major advantage and novelty of our mouse model compared with other available UCP1-KO models (15, 26) is the option to induce conditional Cre-mediated deletion of exon 2 in the UCP1 gene, using tamoxifen- or doxycycline-inducible Cre-systems. Although, we described the constitutive UCP1-KO, this system enables conditional cell

type-specific or age-dependent knockout of UCP1. This is of significance to investigate the role of alternative mechanisms for nonshivering thermogenesis that might be recruited due to the lack of UCP1 in early life stages. So far, the only available inducible model was the UCP1-DTR mouse, expressing the diphtheria toxin receptor (DTR) under control of the UCP1 promoter, thus depleting UCP1-expressing cells (38, 63). This provided first insights about the contribution of brite adipocytes to energy expenditure (63). In contrast, our model will allow the selective ablation of UCP1 in distinct cell types while leaving these cells otherwise functional. Further research on inducible UCP1-KO mice based on our knockout strategy will help to study the recruitment of alternative thermogenic mechanism and to clarify the role of individual thermogenic adipocytes to nonshivering thermogenesis.

In summary, we provide evidence that the abundance of UCP1 does not necessarily influence energy metabolism at thermoneutrality and provide a new mouse model as foundation for a better understanding of the contribution of UCP1 in different cell types or life stages to energy metabolism.

## SUPPLEMENTAL DATA

Supplemental Fig. S1: <https://doi.org/10.6084/m9.figshare.15112227>.

Supplemental Fig. S2: <https://doi.org/10.6084/m9.figshare.15112233>.

Supplemental Fig. S3: <https://doi.org/10.6084/m9.figshare.15112236>.

Supplemental Fig. S4: <https://doi.org/10.6084/m9.figshare.17088992>.

Supplemental Fig. S5: <https://doi.org/10.6084/m9.figshare.15112245>.

## ACKNOWLEDGMENTS

We thank the animal caretakers for support with animal work. We thank Katherina Schnabl for excellent technical support with the indirect calorimetry as well as Johanna Bruder and Josef Oeckl for assisting during tissue sampling.

Present address of R. Kühn: Center for Molecular Medicine in the Helmholtz Association, Berlin, Germany.

## GRANTS

This work was financed by the “Nutribrite” grant [Deutsche Forschungsgemeinschaft (DFG) #KL973/13-1 and French Agence Nationale de la Recherche #ANR-15-CE14-0033], the DFG funded Collaborative Research Center CRC1371:P13, and the Else Kröner Fresenius Foundation (EKFS) (to M. Klingenspor), as well as a European Commission Grant EUComm (EU-FP6, LSHM-CT-2005-01893). Contributions by N. Köhler and J. K. Pauling are funded by the Bavarian State Ministry of Science and the Arts within the framework of the Bavarian Research Institute for Digital Transformation (bidt). J. Heeren was supported by a DFG grant with the project-ID: 335447727 - SFB 1328. A. Worthmann, J. Heeren, and M. Klingenspor are members of the transregio collaborative research center ‘BATenergy’ funded by DFG (TRR333/1; project# 450149205).

## DISCLOSURES

No conflicts of interest, financial or otherwise, are declared by the authors.



## AUTHOR CONTRIBUTIONS

S.D., M.W., and M.K. conceived and designed research; S.D., S.F.M., A.W., and M.M.F. performed experiments; S.D., A.S., N.K., and J.K.P. analyzed data; S.D., A.S., N.K., J.K.P., and M.K. interpreted results of experiments; S.D. and A.S. prepared figures; S.D. drafted manuscript; S.D., A.S., S.F.M., W.W., S.M., M.H.d.A., R.K., A.W., M.M.F., J.H., N.K., J.K.P., and M.K. edited and revised manuscript; S.D., A.S., M.W., S.F.M., W.W., S.M., M.H.d.A., R.K., A.W., M.M.F., J.H., N.K., J.K.P., and M.K. approved final version of manuscript.

## REFERENCES

- Klingenspor M. Cold-induced recruitment of brown adipose tissue thermogenesis. *Exp Physiol* 88: 141–148, 2003. doi:10.1113/eph8802508.
- Bartelt A, Bruns OT, Reimer R, Hohenberg H, Ittrich H, Peldschus K, Kaul MG, Tromsdorf UI, Weller H, Waurisch C, Eychmüller A, Gordts PLSM, Rinninger F, Bruegelmann K, Freund B, Nielsen P, Merkel M, Heeren J. Brown adipose tissue activity controls triglyceride clearance. *Nat Med* 17: 200–206, 2011. doi:10.1038/nm.2297.
- Fromme T, Klingenspor M. Uncoupling protein 1 expression and high-fat diets. *Am J Physiol Regul Integr Comp Physiol* 300: R1–R8, 2011. doi:10.1152/ajpregu.00411.2010.
- Rothwell NJ, Stock MJ. A role for brown adipose tissue in diet-induced thermogenesis. *Obes Res* 5: 650–656, 1997. doi:10.1002/j.1550-8528.1997.tb00591.x.
- Glick Z, Teague RJ, Bray GA. Brown adipose tissue: thermic response increased by a single low protein, high carbohydrate meal. *Science* 213: 1125–1127, 1981. doi:10.1126/science.7268419.
- Li Y, Schnabl K, Gabler SM, Willershäuser M, Reber J, Karlas A, Laurila S, Lahesmaa M, U Din M, Bast-Habersbrunner A, Virtanen KA, Fromme T, Bolze F, O'Farrell LS, Alsina-Fernandez J, Coskun T, Ntzachristos V, Nuutila P, Klingenspor M. Secretin-activated brown fat mediates prandial thermogenesis to induce satiation. *Cell* 175: 1561–1574.e12, 2018. doi:10.1016/j.cell.2018.10.016.
- Laurila S, Sun L, Lahesmaa M, Schnabl K, Laitinen K, Klén R, Li Y, Balaz M, Wolfrum C, Steiger K, Niemi T, Taittonen M, U-Din M, Välikangas T, Elo LL, Eskola O, Kirjavainen AK, Nummenmaa L, Virtanen KA, Klingenspor M, Nuutila P. Secretin activates brown fat and induces satiation. *Nat Metab* 3: 798–809, 2021. doi:10.1038/s42255-021-00409-4.
- Schnabl K, Li Y, U-Din M, Klingenspor M. Secretin as a satiation whisperer with the potential to turn into an obesity-curbing knight. *Endocrinology* 162: bqab113, 2021. doi:10.1210/endo/bqab113.
- Gnad T, Scheibler S, von Kügelgen I, Scheele C, Kilić A, Glöde A, Hoffmann LS, Reverte-Salisa L, Horn P, Mutlu S, El-Tayeb A, Kranz M, Deuther-Conrad W, Brust P, Lidell ME, Betz MJ, Enerbäck S, Schrader J, Yegutkin GG, Müller CE, Pfeifer A. Adenosine activates brown adipose tissue and recruits beige adipocytes via A2A receptors. *Nature* 516: 395–399, 2014. doi:10.1038/nature13816.
- Zietak M, Kozak LP. Bile acids induce uncoupling protein 1-dependent thermogenesis and stimulate energy expenditure at thermoneutrality in mice. *Am J Physiol Endocrinol Physiol* 310: E346–E354, 2016. doi:10.1152/ajpendo.00485.2015.
- Scheele C, Wolfrum C. Brown adipose crosstalk in tissue plasticity and human metabolism. *Endocr Rev* 41: 53–65, 2020. doi:10.1210/endo/bnz007.
- Becher T, Palanisamy S, Kramer DJ, Eljalby M, Marx SJ, Wibmer AG, Butler SD, Jiang CS, Vaughan R, Schöder H, Mark A, Cohen P. Brown adipose tissue is associated with cardiometabolic health. *Nat Med* 27: 58–65, 2021. doi:10.1038/s41591-020-1126-7.
- Kajimura S, Spiegelman BM, Seale P. Brown and beige fat: physiological roles beyond heat generation. *Cell Metab* 22: 546–559, 2015. doi:10.1016/j.cmet.2015.09.007.
- Fischer AW, Cannon B, Nedergaard J. Optimal housing temperatures for mice to mimic the thermal environment of humans: an experimental study. *Mol Metab* 7: 161–170, 2018. doi:10.1016/j.molmet.2017.10.009.
- Bond LM, Ntambi JM. UCP1 deficiency increases adipose tissue monounsaturated fatty acid synthesis and trafficking to the liver. *J Lipid Res* 59: 224–236, 2018. doi:10.1194/jlr.M078469.
- Keipert S, Lutter D, Schroeder BO, Brandt D, Ståhlman M, Schwarzmayr T, Graf E, Fuchs H, de Angelis MH, Tschöp MH, Rozman J, Jastroch M. Endogenous FGF21-signaling controls paradoxical obesity resistance of UCP1-deficient mice. *Nat Commun* 11: 624, 2020 [Erratum in *Nat Commun* 12: 1804, 2021]. doi:10.1038/s41467-019-14069-2.
- Liu X, Rossmeisl M, McClaine J, Riachi M, Harper M-E, Kozak LP. Paradoxical resistance to diet-induced obesity in UCP1-deficient mice. *J Clin Invest* 111: 399–407, 2003 [Erratum in *J Clin Invest* 111: 759, 2003]. doi:10.1172/jci15737.
- Wang T, Wang Y, Kontani Y, Kobayashi Y, Sato Y, Mori N, Yamashita H. Evodiamine improves diet-induced obesity in a uncoupling protein-1-independent manner: Involvement of antiadipogenic mechanism and extracellularly regulated kinase/mitogen-activated protein kinase signaling. *Endocrinology* 149: 358–366, 2008. doi:10.1210/en.2007-0467.
- Tremaroli V, Bäckhed F. Functional interactions between the gut microbiota and host metabolism. *Nature* 489: 242–249, 2012. doi:10.1038/nature11552.
- Zieötak M, Kovatcheva-Datchary P, Markiewicz LH, Ståhlman M, Kozak LP, Bäckhed F. Altered microbiota contributes to reduced diet-induced obesity upon cold exposure. *Cell Metab* 23: 1216–1223, 2016. doi:10.1016/j.cmet.2016.05.001.
- Wu T-R, Lin C-S, Chang C-J, Lin T-L, Martel J, Ko Y-F, Ojcius DM, Lu C-C, Young JD, Lai H-C. Gut commensal *Parabacteroides goldsteinii* plays a predominant role in the anti-obesity effects of polysaccharides isolated from *Hirsutiella sinensis*. *Gut* 68: 248–262, 2019. doi:10.1136/gutjnl-2017-315458.
- Chevalier C, Stojanović O, Colin DJ, Suarez-Zamorano N, Tarallo V, Veyrat-Durebex C, Rigo D, Fabbiano S, Stevanović A, Hagemann S, Montet X, Seimille Y, Zamboni N, Hapfelmeier S, Trajkovski M. Gut microbiota orchestrates energy homeostasis during cold. *Cell* 163: 1360–1374, 2015. doi:10.1016/j.cell.2015.11.004.
- Krisko TI, Nicholls HT, Bare CJ, Holman CD, Putzel GG, Jansen RS, Sun N, Rhee KY, Banks AS, Cohen DE. Dissociation of adaptive thermogenesis from glucose homeostasis in microbiome-deficient mice. *Cell Metab* 31: 592–604.e9, 2020. doi:10.1016/j.cmet.2020.01.012.
- Li G, Xie C, Lu S, Nichols RG, Tian Y, Li L, Patel D, Ma Y, Brocker CN, Yan T, Krausz KW, Xiang R, Gavrilova O, Patterson AD, Gonzalez FJ. Intermittent fasting promotes white adipose browning and decreases obesity by shaping the gut microbiota. *Cell Metab* 26: 672–685.e4, 2017. doi:10.1016/j.cmet.2017.08.019.
- Anunciado-Koza R, Ukropec J, Koza RA, Kozak LP. Inactivation of UCP1 and the glycerol phosphate cycle synergistically increases energy expenditure to resist diet-induced obesity. *J Biol Chem* 283: 27688–27697, 2008. doi:10.1074/jbc.M804268200.
- Enerbäck S, Jacobsson A, Simpson EM, Guerra C, Yamashita H, Harper ME, Kozak LP. Mice lacking mitochondrial uncoupling protein are cold-sensitive but not obese. *Nature* 387: 90–94, 1997. doi:10.1038/387090a0.
- Maurer SF, Fromme T, Mocek S, Zimmermann A, Klingenspor M. Uncoupling protein 1 and the capacity for nonshivering thermogenesis are components of the glucose homeostatic system. *Am J Physiol Endocrinol Physiol* 318: E198–E215, 2020. doi:10.1152/ajpendo.00121.2019.
- Winn NC, Vieira-Potter VJ, Gastecki ML, Welly RJ, Scroggins RJ, Zidon TM, Gaines TL, Woodford ML, Karasheva NG, Kanaley JA, Sacks HS, Padilla J. Loss of UCP1 exacerbates western diet-induced glycemic dysregulation independent of changes in body weight in female mice. *Am J Physiol Regul Integr Comp Physiol* 312: R74–R84, 2017. doi:10.1152/ajpregu.00425.2016.
- Feldmann HM, Golozoubova V, Cannon B, Nedergaard J. UCP1 ablation induces obesity and abolishes diet-induced thermogenesis in mice exempt from thermal stress by living at thermoneutrality. *Cell Metab* 9: 203–209, 2009. doi:10.1016/j.cmet.2008.12.014.
- Rowland LA, Maurya SK, Bal NC, Kozak L, Periasamy M. Sarcolipin and uncoupling protein 1 play distinct roles in diet-induced thermogenesis and do not compensate for one another. *Obesity (Silver Spring)* 24: 1430–1433, 2016. doi:10.1002/oby.21542.
- von Essen G, Lindsund E, Cannon B, Nedergaard J. Adaptive facultative diet-induced thermogenesis in wild-type but not in UCP1-ablated mice. *Am J Physiol Endocrinol Physiol* 313: E515–E527, 2017. doi:10.1152/ajpendo.00097.2017.

32. Luijten IHN, Feldmann HM, von Essen G, Cannon B, Nedergaard J. In the absence of UCP1-mediated diet-induced thermogenesis, obesity is augmented even in the obesity-resistant 129S mouse strain. *Am J Physiol Endocrinol Physiol* 316: E729–E740, 2019. doi:10.1152/ajpendo.00020.2019.
33. Pahlavani M, Ramalingam L, Miller EK, Scoggins S, Menikdiwela KR, Kalupahana NS, Festuccia WT, Moustaid-Moussa N. Eicosapentaenoic acid reduces adiposity, glucose intolerance and increases oxygen consumption independently of uncoupling protein 1. *Mol Nutr Food Res* 63: 1800821, 2019. doi:10.1002/mnfr.201800821.
34. Wang H, Willershäuser M, Li Y, Fromme T, Schnabl K, Bast-Habersbrunner A, Ramisch S, Mocek S, Klingenspor M. Uncoupling protein-1 expression does not protect mice from diet-induced obesity. *Am J Physiol Endocrinol Physiol* 320: E333–E345, 2021. doi:10.1152/ajpendo.00285.2020.
35. Chen HF, Hsu CM, Huang YS. CPEB 2-dependent translation of long 3'-UTR Ucp1 mRNA promotes thermogenesis in brown adipose tissue. *EMBO J* 37: e99071, 2018. doi:10.15252/embj.201899071.
36. Wang H, Willershäuser M, Karlas A, Gorpas D, Reber J, Ntziachristos V, Maurer S, Fromme T, Li Y, Klingenspor M. A dual Ucp1 reporter mouse model for imaging and quantitation of brown and brite fat recruitment. *Mol Metab* 20: 14–27, 2019. doi:10.1016/j.molmet.2018.11.009.
37. Lowell BB, S-Susulic V, Hamann A, Lawitts JA, Himms-Hagen J, Boyer BB, Kozak LP, Flier JS. Development of obesity in transgenic mice after genetic ablation of brown adipose tissue. *Nature* 366: 740–742, 1993. doi:10.1038/366740a0.
38. Rosenwald M, Perdikari A, Rülcke T, Wolfrum C. Bi-directional interconversion of brite and white adipocytes. *Nat Cell Biol* 15: 659–667, 2013. doi:10.1038/ncb2740.
39. Pettitt SJ, Liang Q, Rairdan XY, Moran JL, Prosser HM, Beier DR, Lloyd KC, Bradley A, Skarnes WC. Agouti C57BL/6N embryonic stem cells for mouse genetic resources. *Nat Methods* 6: 493–495, 2009. doi:10.1038/nmeth.1342.
40. Skarnes WC, Rosen B, West AP, Koutsourakis M, Bushell W, Iyer V, Mujica AO, Thomas M, Harrow J, Cox T, Jackson D, Severin J, Biggs P, Fu J, Nefedov M, De Jong PJ, Stewart AF, Bradley A. A conditional knockout resource for the genome-wide study of mouse gene function. *Nature* 474: 337–344, 2011. doi:10.1038/nature10163.
41. Maurer SF, Fromme T, Grossman LI, Hüttemann M, Klingenspor M. The brown and brite adipocyte marker Cox7a1 is not required for non-shivering thermogenesis in mice. *Sci Rep* 5: 17704, 2015. doi:10.1038/srep17704.
42. Heldmaier G. Metabolic and thermoregulatory responses to heat and cold in the Djungarian hamster, *Phodopus sungorus*. *J Comp Physiol B* 102: 115–122, 1975. doi:10.1007/BF00691297.
43. Fromme T, Hüttinger K, Maurer S, Li Y, Gantert T, Fiamoncini J, Daniel H, Westphal S, Klingenspor M. Bile acid supplementation decreases body mass gain in C57BL/6J but not 129S6/SvEvTac mice without increasing energy expenditure. *Sci Rep* 9: 131, 2019. doi:10.1038/s41598-018-37464-z.
44. Klindworth A, Pruesse E, Schweer T, Peplies J, Quast C, Horn M, Glöckner FO. Evaluation of general 16S ribosomal RNA gene PCR primers for classical and next-generation sequencing-based diversity studies. *Nucleic Acids Res* 41: e1, 2013. doi:10.1093/nar/gks080.
45. Edgar RC. UPARSE: highly accurate OTU sequences from microbial amplicon reads. *Nat Methods* 10: 996–998, 2013. doi:10.1038/nmeth.2604.
46. Lagkouravdos I, Joseph D, Kapfhammer M, Giritli S, Horn M, Haller D, Clavel T. IMNGS: a comprehensive open resource of processed 16S rRNA microbial profiles for ecology and diversity studies. *Sci Rep* 6: 33721–33729, 2016. doi:10.1038/srep33721.
47. Lagkouravdos I, Fischer S, Kumar N, Clavel T. Rhea: a transparent and modular R pipeline for microbial profiling based on 16S rRNA gene amplicons. *PeerJ* 5: e2836, 2017. doi:10.7717/peerj.2836.
48. McMurdie PJ, Holmes S. Waste not, want not: why rarefying microbiome data is inadmissible. *PLoS Comput Biol* 10: e1003531, 2014. doi:10.1371/journal.pcbi.1003531.
49. Quast C, Pruesse E, Yilmaz P, Gerken J, Schweer T, Yarza P, Peplies J, Glöckner FO. The SILVA ribosomal RNA gene database project: improved data processing and web-based tools. *Nucleic Acids Res* 41: D590–D596, 2013. doi:10.1093/nar/gks1219.
50. Yoon SH, Ha SM, Kwon S, Lim J, Kim Y, Seo H, Chun J. Introducing EzBioCloud: a taxonomically united database of 16S rRNA gene sequences and whole-genome assemblies. *Int J Syst Evol Microbiol* 67: 1613–1617, 2017. doi:10.1099/ijsem.0.001755.
51. Schneider BB, Covey TR, Coy SL, Krylov EV, Nazarov EG. Planar differential mobility spectrometer as a pre-filter for atmospheric pressure ionization mass spectrometry. *Int J Mass Spectrom* 298: 45–54, 2010. doi:10.1016/j.jms.2010.01.006.
52. Lintonen TPI, Baker PRS, Suoniemi M, Ubhi BK, Koistinen KM, Duchoslav E, Campbell JL, Ekroos K. Differential mobility spectrometry-driven shotgun lipidomics. *Anal Chem* 86: 9662–9669, 2014. doi:10.1021/ac5021744.
53. Argelaguet R, Arnol D, Bredikhin D, Deloro Y, Velten B, Marioni JC, Stegle O. MOFA+: a statistical framework for comprehensive integration of multi-modal single-cell data. *Genome Biol* 21: 111, 2020. doi:10.1186/s13059-020-02015-1.
54. Argelaguet R, Velten B, Arnol D, Dietrich S, Zenz T, Marioni JC, Buettner F, Huber W, Stegle O. Multi-omics factor analysis—a framework for unsupervised integration of multi-omics data sets. *Mol Syst Biol* 14: e8124, 2018. doi:10.15252/msb.20178124.
55. Singh A, Shannon CP, Gautier B, Rohart F, Vacher M, Tebbutt SJ, Lê Cao K-A. DIABLO: an integrative approach for identifying key molecular drivers from multi-omics assays. *Bioinformatics* 35: 3055–3062, 2019. doi:10.1093/bioinformatics/bty1054.
56. Rohart F, Gautier B, Singh A, Lê Cao K-A. mixOmics: an R package for 'omics feature selection and multiple data integration. *PLOS Comput Biol* 13: e1005752, 2017. doi:10.1371/journal.pcbi.1005752.
57. Heine M, Fischer AW, Schlein C, Jung C, Straub LG, Gottschling K, Mangels N, Yuan Y, Nilsson SK, Liebscher G, Chen O, Schreiber R, Zechner R, Scheja L, Heeren J. Lipolysis triggers a systemic insulin response essential for efficient energy replenishment of activated brown adipose tissue in mice. *Cell Metab* 28: 644–655.e4, 2018. doi:10.1016/j.cmet.2018.06.020.
58. Schoeller M, Caesar R. Dietary lipids, gut microbiota and lipid metabolism. *Rev Endocr Metab Disord* 20: 461–472, 2019. doi:10.1007/s11154-019-09512-0.
59. Granneman JG, Burnazi M, Zhu Z, Schwamb LA. White adipose tissue contributes to UCP1-independent thermogenesis. *Am J Physiol Endocrinol Physiol* 285: E1230–E1236, 2003. doi:10.1152/ajpendo.00197.2003.
60. Meyer CW, Willershäuser M, Jastroch M, Rourke BC, Fromme T, Oelkrug R, Heldmaier G, Klingenspor M. Adaptive thermogenesis and thermal conductance in wild-type and UCP1-KO mice. *Am J Physiol Regul Integr Comp Physiol* 299: R1396–R1406, 2010. doi:10.1152/ajpregu.00021.2009.
61. Bachman ES, Dhillon H, Zhang CY, Cinti S, Bianco AC, Kobilka BK, Lowell BB.  $\beta$ AR signaling required for diet-induced thermogenesis and obesity resistance. *Science* 297: 843–845, 2002. doi:10.1126/science.1073160.
62. Rothwell NJ, Stock MJ. A role for brown adipose tissue in diet-induced thermogenesis. *Nature* 281: 31–35, 1979. doi:10.1038/281031a0.
63. Challa TD, Dapito DH, Kulenkampff E, Kiehlmann E, Moser C, Straub L, Sun W, Wolfrum C. A genetic model to study the contribution of brown and brite adipocytes to metabolism. *Cell Rep* 30: 3424–3433.e4, 2020. doi:10.1016/j.celrep.2020.02.055.